Agricultural Water Management 277 (2023) 108089

Contents lists available at ScienceDirect

Agricultural Water Management

journal homepage: www.elsevier.com/locate/agwat

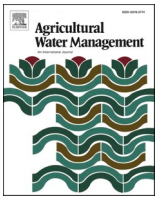

# Assessing the sensitive spectral bands for soybean water status monitoring and soil moisture prediction using leaf-based hyperspectral reflectance

Luís Guilherme Teixeira Crusiol [a], Marcos Rafael Nanni [b], Renato Herrig Furlanetto [b], Rubson Natal Ribeiro Sibaldelli [a], Liang Sun [c,*], Sergio Luiz Gonçalves [a], José Salvador Simonetto Foloni [a], Liliane Marcia Mertz-Henning [a], Alexandre Lima Nepomuceno [a], Norman Neumaier [a], José Renato Bouças Farias [a]

[a] Embrapa Soja (National Soybean Research Center – Brazilian Agricultural Research Corporation), Londrina 86001–970, PR, Brazil
[b] Department of Agronomy, State University of Maringá, Maringá 87020–900, PR, Brazil
[c] Key Laboratory of Agricultural Remote Sensing, Ministry of Agriculture – Institute of Agricultural Resources and Regional Planning, Chinese Academy of Agricultural Sciences, Beijing 100081, China

ARTICLE INFO

Handling editor B.E. Clothier

*Keywords:*
Drought
Leaf water content
Yield
Principal component analysis
Partial least squares regression

ABSTRACT

The stability of soybean yields in Brazil is regularly affected by drought periods, and soil management practices are crucial to expanding the water holding capacity of the soil and providing higher levels of moisture during critical periods, which contribute to increasing crop yields, relieving the need for non-agricultural areas to be converted into croplands. The research reported herein aimed to quantitatively monitor the soil moisture of a soybean crop through leaf-based hyperspectral reflectance and suggest a remote sensing-based approach that might assist in identifying soil management zones. A field experiment at the Brazilian Agricultural Research Corporation during 2016/2017, 2017/2018, and 2018/2019 cropping seasons had ten soybean genotypes subjected to four water conditions: irrigated, non-irrigated, and water deficit induced at the vegetative or reproductive stages. The soil of the experimental site is characterized as Udox Oxisol. Leaf reflectance (400–2500 nm) was collected by the spectroradiometer FieldSpec 3 Jr simultaneously with soil moisture (0–20 and 20–40 cm depths) at eleven dates. Data submitted to Principal Component Analysis (PCA) evaluated the clustering of water conditions and which are the most critical spectral wavelengths to characterize the plant water status. The Partial Least Squares Regression (PLSR) was applied to develop a quantitative spectral model to predict soil moisture. The PCA explained over 93% of the spectral variance within each assessment day, and shortwave infrared wavelengths presented a higher contribution to water status clustering. At the cross-validation step, the PLSR presented $R^2$ up to 0.860 and 0.906 (0–20 and 20–40 cm) underperforming when soil moisture showed no significant differences between water conditions. Using samples from all assessment days, PLSR presented $R^2$ = 0.609 and 0.722 (0–20 and 20–40 cm) at the external validation step (RMSE = 2.7 and 1.9, respectively), with a soil moisture range equal to 16–35% and 20–35% at both depths, remarkably outperforming the traditional univariate spectral models. Our results contribute to soil moisture assessment in extensive soybean areas regardless of the stage of crop development and provide a significant contribution since the Brazilian soybean crop calendar might present differences of over 30 days within the same production region. Due to that, soybean plants are rarely at the same phenological stage on a given date in the season.

## 1. Introduction

According to the Food and Agriculture Organization of the United Nations (Anon, 2018), the world population will exceed 9 billion people by 2050, which requires maximized food production to meet the food demand and assist food security policies. Concurrently to the

* Correspondence to: Institute of Agricultural Resources and Regional Planning, Chinese Academy of Agricultural Sciences, Beijing 100081, China.
*E-mail addresses:* luis.crusiol@colaborador.embrapa.br (L.G.T. Crusiol), mrnanni@uem.br (M.R. Nanni), rubson.sibaldelli@embrapa.br (R.N.R. Sibaldelli), sunliang@caas.cn (L. Sun), sergio.goncalves@embrapa.br (S.L. Gonçalves), salvador.foloni@embrapa.br (J.S.S. Foloni), liliane.henning@embrapa.br (L.M. Mertz-Henning), alexandre.nepomuceno@embrapa.br (A.L. Nepomuceno), norman.neumaier@embrapa.br (N. Neumaier), joserenato.farias@embrapa.br (J.R.B. Farias).

https://doi.org/10.1016/j.agwat.2022.108089
Received 16 August 2022; Received in revised form 30 November 2022; Accepted 1 December 2022

agricultural production expansion, only sustainable practices adoption shall guarantee environmental preservation (Anon, 2018). Hence, increasing crop yield is crucial to relieve the need for non-agricultural areas to be converted into croplands, meet the world food demand, and adopt sustainable production standards (Nepomuceno, 2021).

Brazil is the largest soybean producer, responsible for nearly one-third (140 million tons – Anon, 2022) of soybeans produced worldwide (372 million tons – Anon, 2022). In the last decades, soybean yield in Brazil has grown at higher rates compared to the increment of production areas, which prevented, by the adoption of technologies for soybean production and, consequently, yield gains, millions of ha to be converted into agricultural areas to achieve the same production amount (Gazzoni and Dall'Agnol, 2018). However, the yield stability in Brazil is regularly affected by unfavorable climatic events, especially drought periods. Although dryness is not observable across the entire soybean cropping season, periods of water deficit regularly cause high yield losses, compromising over 30% of the Brazilian soybean production (Sentelhas et al., 2015) and leading to financial losses of over US$79 billion in 38 years (Ferreira, 2016).

Irrigated areas in Brazil represent a small percentage of the areas devoted to agricultural production. Specifically, only about 2% of the areas devoted to soybean production is irrigated (FAO, 2017; CONAB, 2022). Thus, considering the need to optimize the use of water resources (Anon, 2018), several strategies to cope with water deficit periods during the soybean cropping season are available, including but not limited to: the development of soybean cultivars with drought tolerance (Stolf-Moreira et al., 2011; Rolla et al., 2014; Marinho et al., 2016; Honna et al., 2016; Fuganti-Pagliarini et al., 2017); the grouping of soybean production areas, based on their edaphoclimatic characteristics, indicating more suitable cultivars for each of them (Kaster and Farias, 2012); and the agricultural zoning of climatic risk, addressing the more favorable sowing periods for each production area to minimize the probability of occurrence of water deficit periods at critical stages of crop development (Farias et al., 2001). In addition, do Rio et al. (2016) have proposed alternative sowing dates based on the future climatic scenarios for soybean production.

Another strategy is the adoption of soil management practices aiming at enlarging the soil water holding capacity, providing, thus, higher levels of water availability to support crop development during water deficit periods. However, the traditional methods for soil moisture determination are laborious and time-consuming, requiring the collection of several samples in each production area, which impair the soil water status monitoring over large areas in short time intervals. In this context, remote sensing becomes a proxy for crop water status monitoring, delivering accurate, fast, and spatial information about crop conditions non-destructively.

Using remote sensing information, Peng et al. (2013), Xu et al. (2016), and Yuan et al. (2019) have reported the relation between soil moisture and soil spectral response. However, assessing soil moisture via spectral response requires laborious and time-consuming field campaigns for in situ samplings. Therefore, most existing methods using remotely sensed data for monitoring soil moisture rely on the indirect and qualitative relation between crop reflectance and soil moisture, which, in turn, bases itself on the direct relationship between reflectance and vegetation water content. This relation is a crucial indicator of soil water status (Kovar et al., 2019; Zhang et al., 2021).

Many authors demonstrated the relation between reflectance and vegetation water content in several crops, including wheat (El-Hendawy et al., 2014; Feng et al., 2017; Zhang et al., 2021), maize (Ge et al., 2016 and 2019b, Zygielbaum et al., 2009), cotton (Yi et al., 2013; Zhang et al., 2012) and soybean (Kovar et al., 2019; Braga et al., 2021). In soybean, Braga et al. (2021) and Wijewardana et al. (2019) reported that physiological traits, such as photosynthesis, stomatal conductance, transpiration, internal $CO_2$ content, leaf water potential, and leaf water content are affected by low levels of soil moisture. So, spectral measurements can be accurately related to crop traits for monitoring crop and soil water status.

Although the many efforts to retrieve crop water status by spectral measurements, still lack discussion on the direct and quantitative soil moisture assessment through crop reflectance (Ge et al., 2019a). Sobrino et al. (2012) used an airborne hyperspectral scanner (AHS) and satellite images to estimate the soil moisture of several crops at distinct crop phenological stages. Ge et al. (2019a) assessed soil moisture via UAV-based hyperspectral image over wheat fields at a single phenological stage, and Panigrahi and Das (2018) modeled soil water potential using ground-based hyperspectral measurements over rice fields at multiple phenological stages. However, models for soil moisture prediction using canopy spectral data might be susceptible to interferences from canopy structure, leaf area, angle and position, shadow, and background (Liu et al., 2015; Ma et al., 2019), imposing limitations on acquisition of the quantitative relation between soil moisture and leaf reflectance and the extendibility of the developed models to new agricultural areas. Moreover, considering the soybean sowing calendar in Brazil, which might extend over more than one month within the same production area (Crusiol et al., 2021b), it is highly desirable that spectral models accurately predict soil moisture regardless of crop phenological development.

Based on the current progress, this research aims at monitoring the soil moisture quantitatively at 0–20 cm and 20–40 cm depths using leaf-based hyperspectral reflectance to support a soil water holding capacity enlargement through a more precise delimitation of soil management practices in a soybean crop. The specific goals are to assess the sensitive spectral bands for soybean water status monitoring, develop soil moisture prediction models at different stages of crop development, and develop soil moisture prediction models regardless of the soybean crop stage of development.

## 2. Material and methods

### 2.1. Experimental site

The experiment (Fig. 1), in a split-plot model in a randomized complete block design, with four blocks, was undertaken on the experimental farm of the National Soybean Research Center (Embrapa Soja), a branch of the Brazilian Agricultural Research Corporation, located in Londrina Municipality, Paraná State, Southern Brazil (23° 11′ 37″ S, 51° 11′03″ W, 630 m above sea level), in the 2016/2017, 2017/2018 and 2018/2019 cropping seasons, following the soybean production technologies (Embrapa Soja 2013).

The soil of the experimental site (Table 1) is characterized as Udox Oxisol (Anon, 1999), with 75 mm of water holding capacity, with the following characteristics (soil analysis in March 2016):

According to the Köppen climate classification, the experimental site is in a Cfa climate (i.e., subtropical climate), with a mean temperature in the hottest month higher than 22 ºC and rainfall concentrated in the summer months, with no defined dry season (Wrege et al., 2012; Alvares et al., 2013). Considering the soybean calendar in central and south Brazil, the largest soybean producers, the rainy season corresponds to the periods of soybean production, but not without water deficit periods.

The field plots received four water condition treatments: irrigated (IRR, receiving rainfall and irrigation, when necessary, with a soil water matric potential between −0.03 and −0.05 MPa); non-irrigated (NIRR, receiving only rainfall); water deficit induced at the vegetative stages (WDV); water deficit induced at reproductive stages (WDR); and ten soybean genotypes, with drought tolerance genes and different responses to water deficit, were distributed in the subplots: genotypes 1Ea15, 2Ha11, 2Ia4, BR16 and BRS 184 in 2016/2017 and 2017/2018 cropping seasons; and genotypes 1Ea2939, 3Ma2, BRS 283, BRT18–0089 and BRT18–0201 in 2018/2019 cropping season.

Automated rainout shelters kept WDV and WDR subplots free from receiving rainfalls higher than 0.1 mm, in the vegetative and reproductive phases, respectively, and imposed the water deficit treatments,

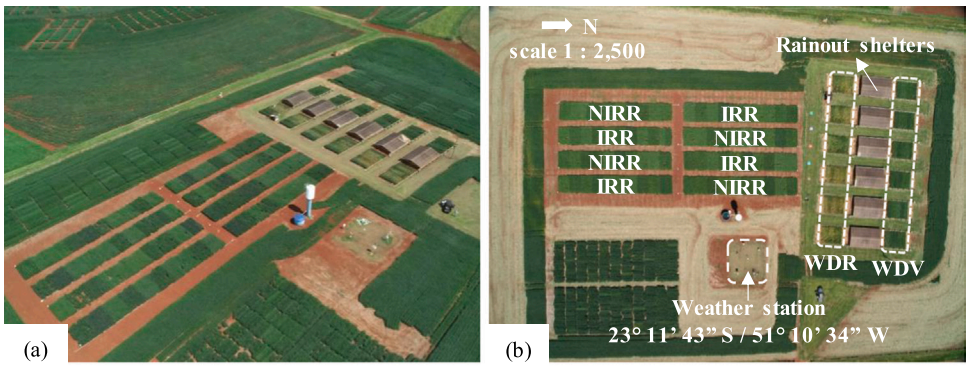


**Fig. 1.** Experimental area overview (a) and description of the weather station and treatment plots (b): irrigated (IRR), non-irrigated (NIRR), and water deficit induced at vegetative (WDV) and reproductive (WDR) stages. RGB image obtained by an UAV carrying a regular digital camera.

**Table 1**
Soil characteristics of the experimental area.

| pH | $H^+$+$Al^{3+}$ | $Al^{3+}$ | $Ca^{2+}$ | $Mg^{2+}$ | $K^+$ | CTC | P | C | SB | V% | Clay |
|---|---|---|---|---|---|---|---|---|---|---|---|
| $H_2O$ | $cmol_c\ dm^{-3}$ | | | | | | $mg\ dm^{-3}$ | $g\ dm^{-3}$ | | | $g\ kg^{-1}$ |
| 4.9 | 3.5 | 0.03 | 3.9 | 1.8 | 0.7 | 10.0 | 24.2 | 15.6 | 6.5 | 64.8 | 710 |

and increased the soil gravimetric humidity variability across treatments. Shelters automatically uncovered plants once rainfalls had ceased. The plots had in their perimeter vertical concrete barriers (buried up to 90 cm depth) to prevent water lateral movement from outside into the plot soil. During the period in which WDV plots were deprived of rainfalls, WDR was under natural water availability conditions. From the flowering period to full maturity (harvesting), the WDR treatment was deprived of natural rainfall and WDV plots began to be rain watered (under natural water availability conditions). Thus, water deficit periods could be simulated both in the vegetative and reproductive stages of development. Drip irrigation was performed using groundwater from artesian well and kept in a water tank.

Table 2 displays the sowing dates and periods of water deficit inducement in the vegetative and reproductive periods. Table 3 presents the irrigation schedule performed in the 2016/2017 and 2018/2019 cropping seasons.

The irrigation volume needed to keep the soil water matric potential between − 0.03 and − 0.05 MPa was determined by the soil moisture (0–20 and 20–40 cm depths) on IRR plots, daily monitored by tensiometers installed on each block. In the 2017/2018 cropping season, there was no need for irrigation, and, therefore, plants of IRR and NIRR treatments were under the same experimental conditions. In the 2016/2017 cropping season, IRR plots received 69.4 mm of irrigation between November 11 and 25. In the 2018/2019 cropping season, IRR plots received irrigation during two periods: between December 6 and 20, 2018 (63 mm) and between January 29 and February 11, 2018 (43.1 mm), in a total of 106.1 mm).

**Table 2**
Sowing dates and periods of inducement of water deficit at the vegetative and reproductive periods during the 2016/2017, 2017/2018, and 2018/2019 cropping seasons.

| Cropping season | Sowing | Water deficit induced at vegetative stages | Water deficit induced at reproductive stages | Harvesting period |
|---|---|---|---|---|
| 2016/2017 | October 19, 2016 | From 37 DAS to 54 DAS | From 54 DAS to the harvesting period | From 116 DAS |
| 2017/2018 | October 18, 2017 | From 33 DAS to 62 DAS | From 62 DAS to the harvesting period | From 139 DAS |
| 2018/2019 | October 16, 2018 | From 41 DAS to 64 DAS | From 64 DAS to 90 DAS | From 119 DAS |

**Table 3**
Irrigation schedule for 2016/2017 and 2018/2019 cropping seasons.

| Cropping season | Days after sowing | Quantity (mm) | Duration (minutes) |
|---|---|---|---|
| 2016/2017 | 24 | 14.4 | 60 |
| | 29 | 4.8 | 20 |
| | 30 | 7.2 | 30 |
| | 31 | 9.6 | 40 |
| | 34 | 4.8 | 20 |
| | 35 | 4.8 | 20 |
| | 36 | 4.8 | 20 |
| | 37 | 4.8 | 20 |
| | 38 | 14.4 | 60 |
| 2018/2019 | 52 | 14.4 | 60 |
| | 53 | 14.4 | 60 |
| | 57 | 11.5 | 48 |
| | 58 | 5.7 | 24 |
| | 59 | 5.7 | 24 |
| | 61 | 8.4 | 35 |
| | 66 | 2.9 | 12 |
| | 106 | 7.2 | 30 |
| | 109 | 8.4 | 35 |
| | 114 | 11.5 | 48 |
| | 115 | 2.9 | 12 |
| | 116 | 8.4 | 35 |
| | 119 | 4.8 | 20 |

In all plots, soil moisture (0–20 and 20–40 cm depths) was monitored by gravimetric analysis on eleven dates across the three cropping seasons, as described in Table 4. In all plots, at 0–20 and 20–40 cm depths, soil samples were collected using a Dutch auger and immediately placed in hermetic aluminum boxes, weighted and placed in the oven at 105° for 48 h to reach constant weight.

The growth stages of the soybean plants were weekly monitored from emergence to maturation according to Fehr and Caviness (1977), and grain yield was calculated and corrected for 13% grain moisture, according to Eq. (1):

$$GY = \frac{(100 - HGM)}{(100 - DGM)} \times HGW \times \frac{10,000}{HPA}, \quad \text{Eq. 1}$$

**Table 4**
Dates of soil moisture assessment across 2016/2017, 2017/2018, and 2018/2019 cropping seasons.

| Cropping season | Date of assessment | Days after sowing |
|---|---|---|
| 2016/2017 | December 16, 2016 | 58 |
| | February 08, 2017 | 112 |
| 2017/2018 | December 14, 2017 | 57 |
| | January 22, 2018 | 96 |
| | February 01, 2018 | 106 |
| | February 07, 2018 | 112 |
| 2018/2019 | November 26, 2018 | 41 |
| | December 12, 2018 | 57 |
| | January 11, 2019 | 87 |
| | January 25, 2019 | 101 |
| | January 31, 2019 | 107 |

in which GY is the grain yield (kg $ha^{-1}$); HGM, the harvested grain moisture (%); DGM, the desired grain moisture (%); HGW, the harvested grain weight (kg); and HPA, the harvested plot area ($m^2$). Harvested grain moisture was measured using the G810 grain moisture meter (Gehaka Inc.).

Weather data – air temperature, relative air humidity, and rainfall – were monitored by the weather station located within the experimental area. The calculation of the climatic water balance was according to Thornthwaite and Mather (1955) for each experimental treatment of each cropping season. Additional information on the weather monitoring of the experiment is available at Sibaldelli and Farias (2017, 2018, 2019).

### 2.2. Spectral data acquisition and processing

Soybean leaf reflectance data was collected by the FieldSpec 3 Jr spectroradiometer (Analytical Spectral Devices, Boulder, CO, USA) with a spectral resolution of 3 nm between 350 and 1400 nm and 30 nm resolution between 1400 and 2500 nm. The output spectra are given in single bands of 1 nm intervals, and 2151 spectral bands (Fig. 2). Each spectral reading was averaged from 20 internal automatic spectral readings, preventing the occurrence of noise in the obtained data.

The plant probe device, connected to the FieldSpec by a one-meter bare fiber (Fig. 2b), was used during the leaf reflectance spectral assessment to prevent illumination interferences of adjacent targets and to ensure pure leaf reflectance spectra collection without noises, scattering, or attenuations from the interaction between electromagnetic energy and atmospheric water vapor. Also, we used an internal 99% reflectance board (Spectralon ®) as the reflectance standard and a 1% reflectance blackboard as the opaque one. The use of the plant probe device does not require the application of spectral filters for noise removal and data smoothness (Streher et al., 2020).

The acquisition of the reflectance spectra data was on the central leaflet of the fullest expanded third trifoliate leaf from the top. Leaf reflectance spectra were collected from four plants and then averaged to minimize spectral variability within the same subplot resulting in the values used for data processing and statistical analysis.

The spectral assessment days coincided with the soil moisture assessment (Table 4), except for December 15, 2016, when the soil moisture was assessed on the day after (December 16, 2016), even though neither irrigation nor rainfall occurred on those dates. A total of 3376 leaf reflectance data were collected, resulting in 844 spectral samples at 11 days of spectral assessment across the three cropping seasons.

The collected leaf reflectance spectra were analyzed within each day of spectral assessment by the hyperspectral reflectance between 400 nm and 2500 nm. Wavelengths between 350 and 399 nm stayed out of the spectral analysis because of the frequent noises observed during vegetation analysis in this spectral interval (Peng et al., 2018; Furlanetto et al., 2021).

### 2.3. Statistical analysis

Upon meeting the assumptions of the analysis of variance (ANOVA), we submitted soil moisture data of the eleven assessments on the three cropping seasons and grain yield data from each cropping season to ANOVA and compared means by the Tukey test ($p \leq 0.05$) using the software Sisvar (Ferreira, 2011).

We used two statistical approaches to monitor the soybean water status and predict soil moisture. The Principal Component Analysis (PCA) explored the qualitative differences in soybean leaf spectral response to investigate the possibility of clustering the water condition treatments. The use of Partial Least Squares Regression (PLSR) was to develop soil moisture prediction models by the soybean leaf-based hyperspectral reflectance. Both PCA and PLSR were performable by The Unscrambler® (CAMO Software - Norway).

#### 2.3.1. Principal Component Analysis – PCA

We applied the Principal Component Analysis to the soybean leaf-based hyperspectral reflectance data within each assessment day (Table 4) to assess the explained variance from leaf-based reflectance and to evaluate whether the clustering of water conditions is possible. The PCA is a data mining method that transforms the full reflectance spectrum into a new group of variables (principal components – PC), using a matrix of covariances composed of all wavelengths. Most of the information on data variance resides in the first principal component (PC1), the second principal component carries the residual information of PC1, the third principal component carries the residual information of PC1 and PC2 (PC1 +PC2), and so on (Jolliffe and Cadima, 2016; Furlanetto et al., 2021).

The PC can be defined as the linear combination of all wavelengths to explain their variance within the dataset. The percentage of explained variance can be assessed by each PC's score, while the contribution of each wavelength to each PC, can be assessed by the loading correlation, expressed in (r).

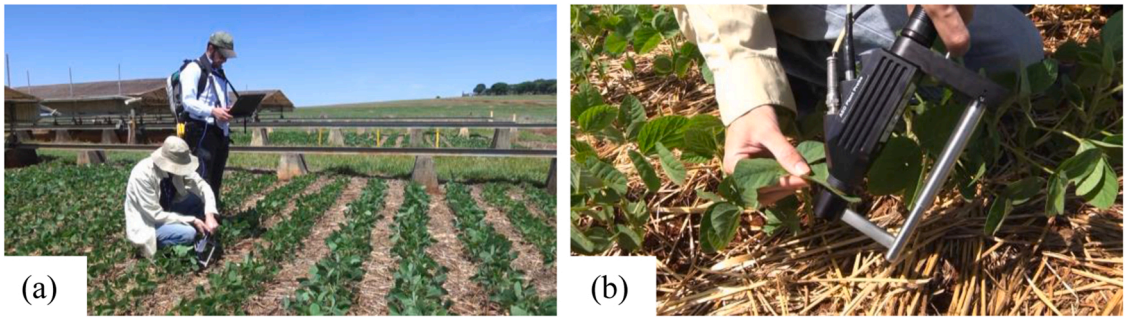


**Fig. 2.** Spectral assessment in the field (a) and detailed view of the plant probe device (b). Photo by Décio de Assis – Embrapa Soja.

#### 2.3.2. Partial Least Squares Regression – PLSR

The Partial Least Squares Regression is a multivariate statistical analysis method widely used when the number of predictor variables (e.g., wavelengths) is larger than the number of response variables (e.g., soil moisture) and has the advantage of overcoming the multicollinearity of independent variables often observed in hyperspectral data (Zhou et al., 2019). Based on a new dataset of latent variables (or PLSR factors or orthogonal base vectors) that account for most of the variation in a trait variable, the spectral data (matrix 'X') is correlated to the soil moisture (matrix 'Y') using a linear model composed by wavelength scaling coefficients derived from the full-spectrum data (Yendrek et al., 2017). The number of PLSR factors, a critical process in the PLSR deeply affecting its prediction capacity (Streher et al., 2020), was set based on the lowest value of root mean square error (RMSE), highest coefficient of determination ($R^2$), and value of Bias close to zero through the "leave-one-out" cross-validation method (Souza et al., 2013). On each spectral dataset, we normalized the reflectance spectra by subtracting the mean reflectance from the actual reflectance at each wavelength, enabling the comparison among the fitted wavelength scaling coefficients. Outliers and homogeneity of the spectral data assessment were by the Leverage and Hotelling's $T^2$ tests.

In the first stage, we used PLSR to develop soil moisture prediction models, at both 0–20 and 20–40 cm depths, by the soybean leaf-based hyperspectral reflectance within each assessment day (Table 4). In the second stage, we evaluated the possibility of developing a soil moisture prediction model based on soybean leaf reflectance at different phenological stages. To do so, PLSR models for soil moisture prediction, at both 0–20 and 20–40 cm depths, were developed using all the 844 samples (leaf reflectance and soil moisture) acquired on the eleven assessment days on the three cropping seasons. This randomly divided dataset had two subsets: calibration/cross-validation steps (containing 80% of data – 669 samples) and external validation (with the remaining 20% of the data – 175 samples).

Each developed PLSR model had its accuracy assessed by the coefficient of determination ($R^2$), the root mean squared error (RMSE), and the systematic error (BIAS) in the calibration and cross-validation (using the leave-one-out cross-validation method) steps. In the second stage, PLSR models developed using 80% of samples and tested over the remaining 20% of samples (external validation) were assessed by the $R^2$ and RMSE between predicted and observed soil moisture values at both depths, 0–20 and 20–40 cm.

#### 2.3.3. Comparison of PLSR performance with traditional univariate spectral models

We used three approaches to investigate whether traditional univariate spectral models might deliver competitive results compared to the PLSR using spectral and soil moisture data from all assessment days from the three cropping seasons. We performed tests using the calibration dataset (containing 80% of data – 669 samples) of soil moisture values (0–20 and 20–40 cm) to check their correlation to (a) reflectance from each one of the 2101 single wavelengths; (b) reflectance resampled to broad multispectral bands (Anon, 2021 – supplementary Table 1) and derived vegetation indices (supplementary Table 2); (c) hyperspectral vegetation indices (HVI), derived from all possible combination between two spectral bands, calculated under a normalized difference vegetation index formula, according to Eq. (2):

$$HVI = \frac{Wavelength_1 - Wavelength_2}{Wavelength_1 + Wavelength_2} \quad \text{Eq. 2}$$

The accuracy was assessed by the coefficient of determination ($R^2$) from the linear regression ($p \leq 0.05$) between soil moisture and: each narrow or broad spectral band; and each multispectral or hyperspectral vegetation index. The linear regression models from the outstanding single wavelength, broad multispectral band or vegetation index, and hyperspectral vegetation index were then applied to the remaining 20% of samples (external validation dataset), and the accuracy was assessed by the $R^2$ and RMSE between the predicted and observed values of soil moisture at both depths, 0–20 and 20–40 cm.

## 3. Results and discussion

### 3.1. Effect of experimental treatments on climatic water balance, soil moisture, and grain yield

Fig. 3 presents the climatic water balance, calculated according to Thornthwaite and Mather (1955), for each experimental treatment of each cropping season.

The efficiency of the experimental treatments in simulating water deficit periods at the vegetative and reproductive stages of plant development are in Fig. 3(a, e, i – at December 1 and 2 10-day periods) and Fig. 3(b, f, j - at December 3 and January 1, 2, and 3 10-day periods) respectively, in the three cropping seasons. Higher deficits can be observable in WDR plants, in contrast to WDV, most likely because of the more extended water withholding period to which plants were submitted.

In the 2016/2017 cropping season, the irrigation performed on IRR plots provided good water availability conditions during November 3 and December 1 10-days periods (Fig. 3d). In the 2018/2019 cropping season, it is possible to observe severe natural water deficit periods during both vegetative and reproductive phases (Fig. 3k), and the irrigated treatment promoted good conditions of water availability during December 1, 2, and 3, January 2 and February 2 10-days periods (Fig. 3l).

Fig. 4 presents the soil moisture in the eleven assessment days across the three evaluated cropping seasons. On all assessment days but at 57 DAS in the 2017/2018 cropping season and 41 DAS in the 2018/2019 cropping season, the experimental treatments produced differences in soil gravimetric humidity at both depths, 0–20 cm and 20–40 cm. Considering the dates of water deficit inducement and the irrigation schedule (Tables 2 and 3), the differences among treatments follow the water availability provided by the treatments. At 41 DAS in the 2018/2019 cropping season, the differences between treatments were undetectable since IRR plots had not received irrigation until that day, and the water deficit in the WDV treatment was not present yet.

The effects of differential water availability on soybean yields in the 2016/2017, 2017/2018, and 2018/2019 cropping seasons are in Fig. 5. The effectiveness of the experimental treatments in promoting differential water availability levels to plants is demonstrated by the intense decreases in yield of WDR treatment, especially during the 2017/2018 and 2018/2019 cropping seasons when its attained productivity was less than half of the other treatments.

Although WDV plants were under water scarcity, they revealed similar yield compared to the non-irrigated treatment and higher yield compared to the WDR treatment, reinforcing that the water deficit during the reproductive stages of plant development is more harmful to yield. Rolla et al. (2014) also reported the similar grain yield of soybean plants subjected to water withholding at vegetative stages and plants under natural rainfall or irrigation.

In the 2016/2017 cropping season, a severe natural water deficit was not observed (Fig. 3c), and the 69.6 mm of irrigation on IRR plots, received between 24 and 38 DAS, did not increased yields. However, when severe natural water deficit occurred across both vegetative and reproductive stages, as it occurred in the 2018/2019 cropping season (Fig. 3k), the irrigated treatment revealed higher grain yields compared to plants receiving only natural rainfall.

### 3.2. Principal Component Analysis of soybean leaf spectral response

We submitted the collected leaf-based hyperspectral data to Principal Component Analysis to explore the qualitative spectral differences among the experimental treatments. The spectral response of soybean genotypes evaluated at 87 DAS in the 2018/2019 cropping season,

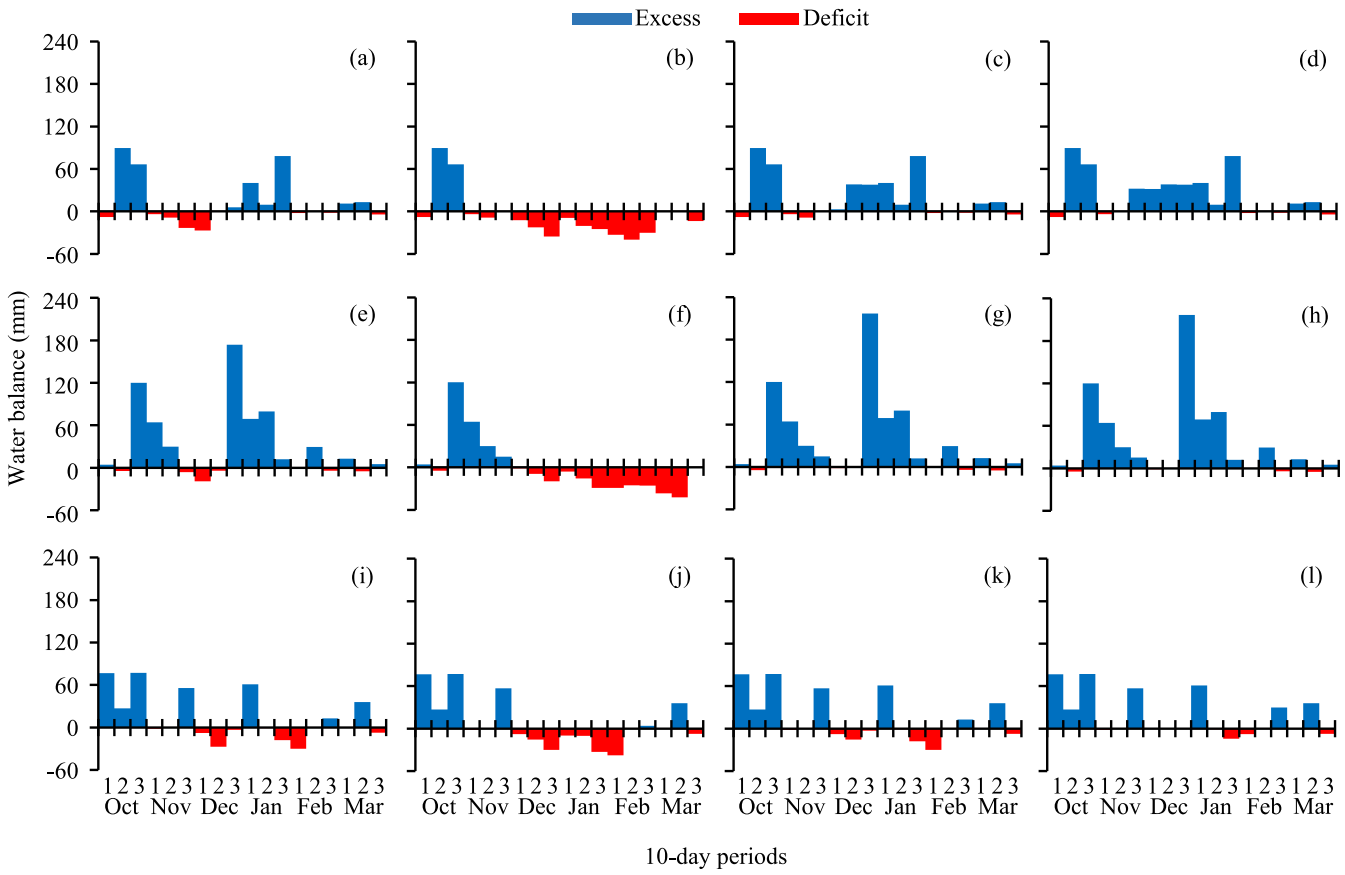


**Fig. 3.** Climatic water balance at 10-day periods in the WDV (a), WDR (b), NIRR (c), and IRR (d) treatments during the 2016/2017 cropping season; WDV (e), WDR (f), NIRR (g) and IRR (h) treatments on 2017/2018 cropping season; WDV (i), WDR (j), NIRR (k) and IRR (l) treatments on 2018/2019 cropping season.

under maximum and minimum soil moisture content at 0–20 cm and 20–40 cm depths, is presented in Fig. 6.

At both depths, it is possible to observe differences in the soybean spectral response across wavelengths, with higher reflectance from plants under lower soil moisture, agreeing with Damm et al. (2018), which described the interference of plant water status in crop spectra. The most conspicuous changes in reflectance due to changes in plant water status were observed across the shortwave infrared spectrum. However, it is worth mentioning that the differences in spectral responses of soybean plants under different levels of water availability are not the same across the wavelengths due to leaf biochemical properties and structure (Maimaitiyiming et al., 2016; Falcioni et al., 2020).

The differential effects of the crop water status on the interaction between electromagnetic energy and soybean leaves across wavelengths can be considered primary or secondary. The primary effects are directly related to the absorption of radiation by water, imposing a strong influence over shortwave infrared (SWIR) wavelengths. The secondary effects cannot be explained solely by the water absorption of radiation but also by its indirect relation to the leaf structure and physiology, imposing a substantial influence over visible and near-infrared wavelengths (Carter, 1991; El-Hendawy et al., 2019).

Visible wavelengths (between 400 nm and 720 nm) are associated with the leaf pigments and the absorption of photosynthetically active radiation and, under water stress, there is lower light absorption, leading to higher values of reflectance (Carter, 1991; Singer et al., 2011; Gitelson et al., 2015; Gitelson, 2019). Near-infrared wavelengths (between 720 and 1300 nm) relate to the light scattering along the mesophyll under the influence of internal leaf structures such as cell wall width, intercellular air spaces, and the amount of mesophyll per unit of leaf area inside the mesophyll (Carter, 1991; Liu et al., 2016, 2020). Hence, changes in crop water status might lead to changes in the internal scattering of the incident light, resulting in higher light absorption and lower reflectance from plants under higher levels of water content.

Between 1300 nm and 2500 nm, the SWIR spectrum demonstrated to be more affected by changes in soil moisture, presenting higher values of reflectance under lower levels of water content. This spectral interval is closely related to leaf water content, one of the critical parameters for establishing the crop water status (Gao, 1996; Wang and Qu, 2007, 2021).

Considering the effects of water availability on leaf reflectance, Fig. 7 presents the results from Principal Component Analysis for each assessment day (Table 4), demonstrating the possibility of clustering the water condition treatments.

For all the eleven evaluation dates across the 2016/2017, 2017/2018, and 2018/2019 cropping seasons, the first PC (PC 1) explained over 44% of the spectral variance within each dataset, and the cumulative percentage of PC 1 and PC 2 demonstrated to be over 82%. The cumulative results from PC1, PC 2, and PC 3 revealed over 93% of the explained variance within each dataset.

In the 2016/2017 cropping season, the scatterplot from PC 1 and PC 2 at 58 DAS (Fig. 7a) showed a similar distribution of the four water condition treatments. By this day, the IRR plots had been receiving 69.4 mm irrigation, and the WDV deprived of 123.8 mm rainfall until flowering (55 DAS), receiving 3.8 mm within three days before the spectral assessment. At 112 DAS, WDR had been deprived of 407.4 mm rainfall since flowering (55 DAS), leading to its distinct spectral response, as demonstrated by Fig. 7(b). On this day, the three other water condition treatments showed similar responses.

In the 2017/2018 cropping season, when WDV had been deprived of 71.4 mm rainfall, the scatterplot from PC 1 and PC 2 at 57 DAS demonstrated similar distribution among the four water condition treatments (Fig. 7c). However, as observed in the previous cropping

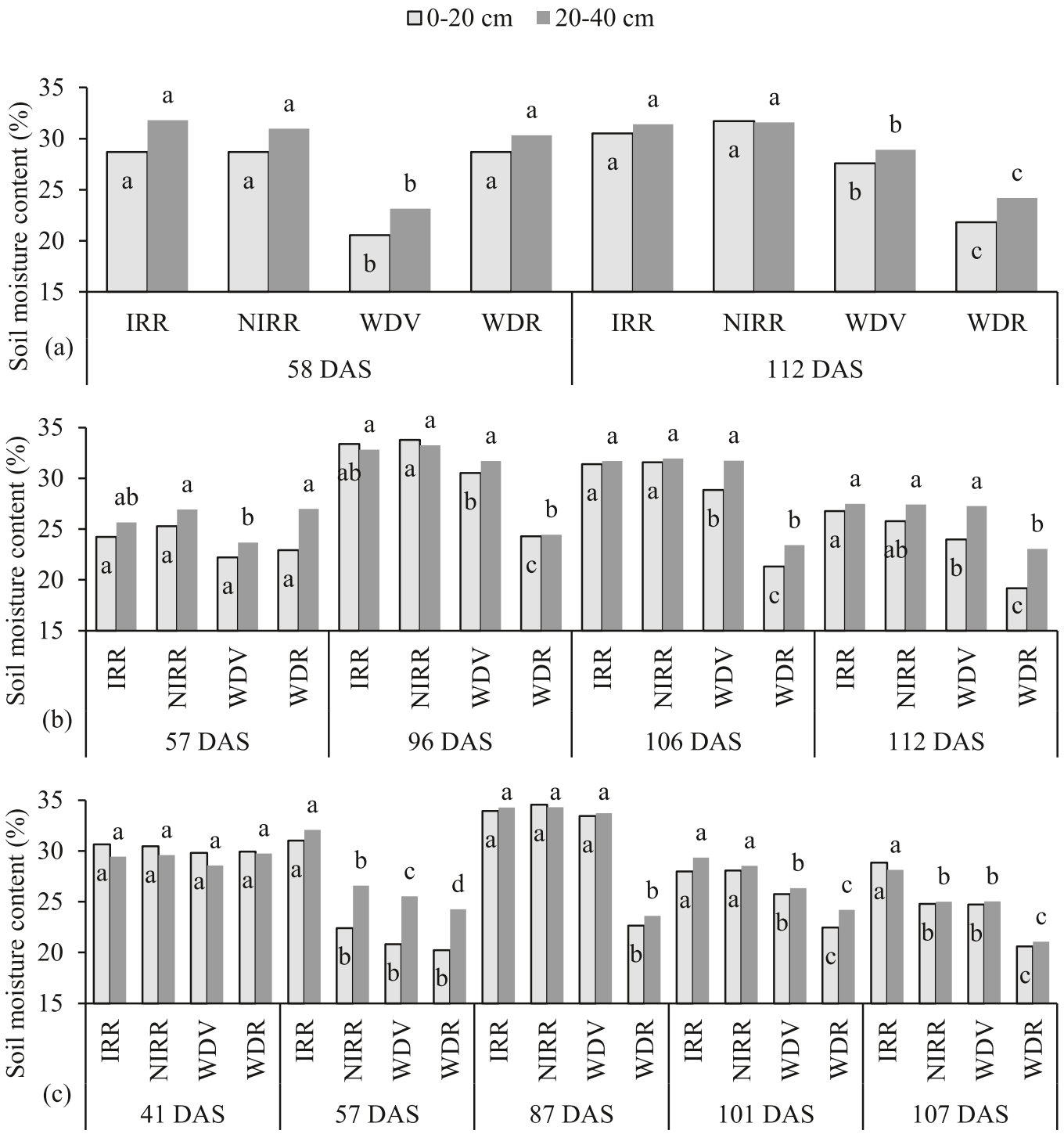


**Fig. 4.** Soil moisture content (%) at 0–20 cm and 20–40 cm depths in the 2016–2017 (a), 2017/2018 (b) and 2018/2019 (c) cropping seasons. Means followed by the same letter among treatments within each depth and on each date do not differ by Tukey test ($p \leq 0.05$).

season, the WDR plots subjected to water scarcity presented a distinct response from the other treatments at 96, 106, and 112 DAS (Fig. 7d, e, f). As for these three assessment dates, the WDR plots had been deprived of 507.9 mm rainfall until 96 DAS and 562.7 mm until 106 and 112 DAS.

In the 2018/2019 cropping season, the four water condition treatments demonstrated similar distribution at 41 DAS when WDV plots had not received the water deficit treatment yet, and the IRR plots had not been irrigated still (Fig. 7g). At 57 DAS (Fig. 7h), the four treatments demonstrated similar responses, regardless of the irrigation performed on IRR (40.3 mm) and the low amount of rain (1.4 mm) prevented to fall on WDV.

As seen in the previous two cropping seasons, the water shortage in WDR is better identifiable by its leaf reflectance analyzed through PCA. At 87 DAS (Fig. 7i), despite the irrigation received (63 mm), the IRR could not be clearly identified in the scatterplot between PC 1 and PC 2. Notwithstanding, the WDR, deprived of 137.4 mm of rainfall, could be undoubtedly clustered from the others. At 101 DAS (Fig. 7j), WDR had been deprived of 143.6 mm of rainwater until 90 DAS (when this treatment started to be rain watered), received 19.8 mm of rainfall since then, which affected the spectral response from this treatment and led to

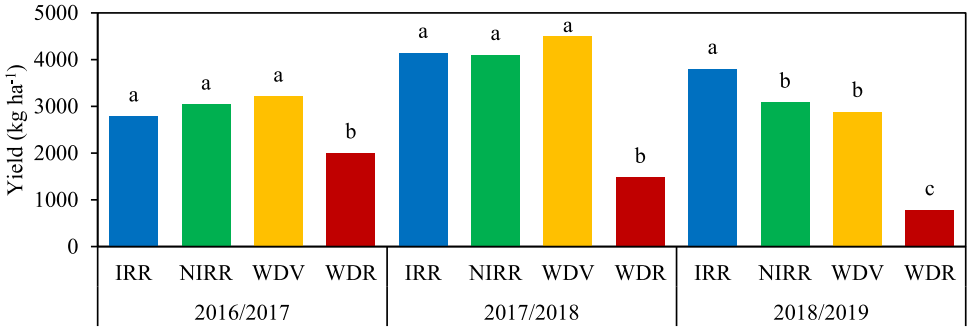


**Fig. 5.** Grain yield in the 2016/2017, 2017/2018 and 2018/2019 cropping seasons (kg ha$^{-1}$). Means followed by the same letter within each cropping season do not differ by Tukey test ($p \leq 0.05$).

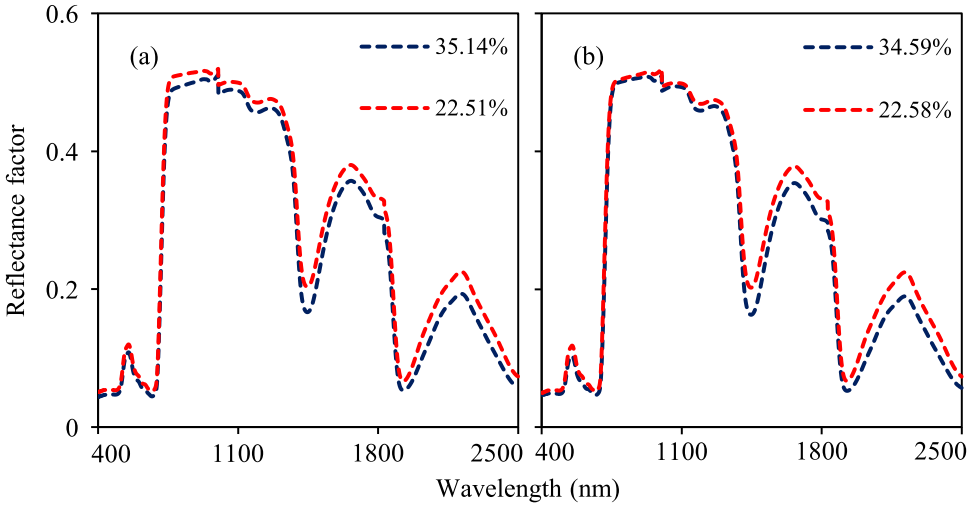


**Fig. 6.** Spectral response of soybean genotypes under maximum and minimum soil moisture content at 0–20 cm (a) and 20–40 cm (b) depths at 87 DAS on the 2018/2019 cropping season.

its clustering concerning the other three water conditions. At 107 DAS (Fig. 7k), IRR could not be clustered out from the other three treatments, although it had received 70.2 mm of total irrigation. WDR, which had received 23.4 mm of rainfall since it started to be rain watered (90 DAS, been previously deprived of 143.6 mm of rainfall), demonstrated differential spectral response relative to the other three water conditions.

As observed in the three cropping seasons, WDR could be better identified (compared to WDV) due to its more extended water deficit period (Table 2) and the consequent impact on the climatic water balance (Fig. 3). Accordingly, as shown in Fig. 5, WDV demonstrated a similar yield to NIRR, while WDR largely impaired yield. Despite the irrigation performed on IRR plots (69.4 mm across the 2016/2017 cropping season and 106.1 mm across the 2018/2019 cropping season), this treatment did not present spectral behavior that could lead to its cluster from the other three water conditions.

Considering the explanatory power from the first three principal components on the eleven spectral assessments for soybean water status monitoring, Fig. 8 presents the loading correlation from the PCA performed across the 2016/2017, 2017/2018, and 2018/2019 cropping seasons. The results revealed three trends in most of the eleven spectral datasets: SWIR wavelengths were the main contributors to the first principal component, NIR wavelengths were the major contributors to the second principal component, and the VIS wavelengths were the predominant contributors to the third principal component.

In the 2016/2017 cropping season, at 112 DAS (Fig. 8b), VIS wavelengths showed a higher contribution to PC 2, while NIR wavelengths contributed mainly to PC 3. That might be associated with changes in leaf structure and photosynthetically active radiation absorption when plants are about to reach the maturation stages of crop development, as highlighted in Crusiol et al. (2021a). In the 2018/2019 cropping season, at 41 DAS (Fig. 8g), NIR wavelengths demonstrated a higher contribution to PC 1, while SWIR wavelengths showed a higher contribution to PC 2. On this date (41 DAS), the four water condition treatments were under the same water status since IRR irrigation had not happened yet, and WDV was still not subjected to water deficit, presenting similar soil moisture contents (Fig. 4c).

### 3.3. *Partial Least Squares Regression for soil moisture prediction by soybean leaf spectral response*

The results of PLSR in the prediction of soil moisture for 2016/2017, 2017/2018, and 2018/2019 cropping seasons are in Table 5. On all days of spectral assessment, one observes higher correlation coefficients ($R^2$) at the calibration step and, consequently, higher values of RMSE at the cross-validation step.

The lowest soil moisture prediction accuracies, both at 0–20 and 20–40 depths, were obtained at 57 DAS in the 2017/2018 cropping season and 41 DAS in the 2018/2019 cropping season. At 57 DAS (2017/2018 cropping season) the coefficients of determination ($R^2$) at 0–20 cm depth were 0.332 (calibration) and 0.230 (cross-validation), while the values of $R^2$ at 20–40 depth were 0.602 (calibration) and 0.492 (cross-validation). At 41 DAS (2018/2019 cropping season), the values of $R^2$ at 0–20 cm depths were 0.308 (calibration) and 0.212 (cross-validation), while the values of $R^2$ at 20–40 depth was 0.006 (calibration) and presented non-significance in the cross-validation step.

The results obtained at the two days (41 and 57 DAS) are related to

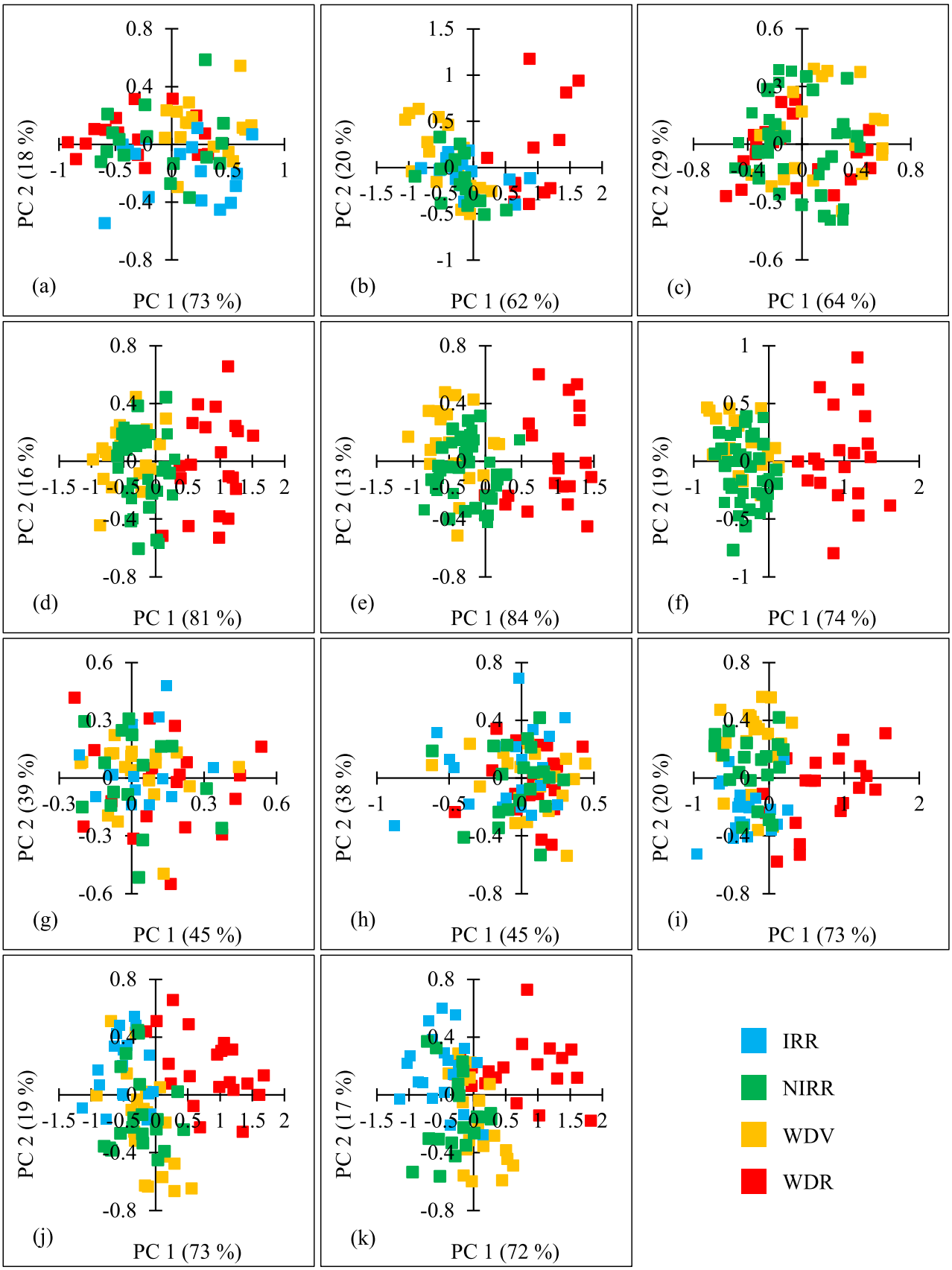


**Fig. 7.** Principal component analysis of the spectral response of soybean crop under the evaluated water conditions in the: 2016/2017 cropping season at 57 DAS (a) and 112 DAS (b); 2017/2018 cropping season at 57 DAS (c), 96 DAS (d), 106 DAS (e) and 112 DAS (f); 2018/2019 cropping season at 41 DAS (g), 57 DAS (h), 87 DAS (i), 101 DAS (j) and 107 DAS (k).

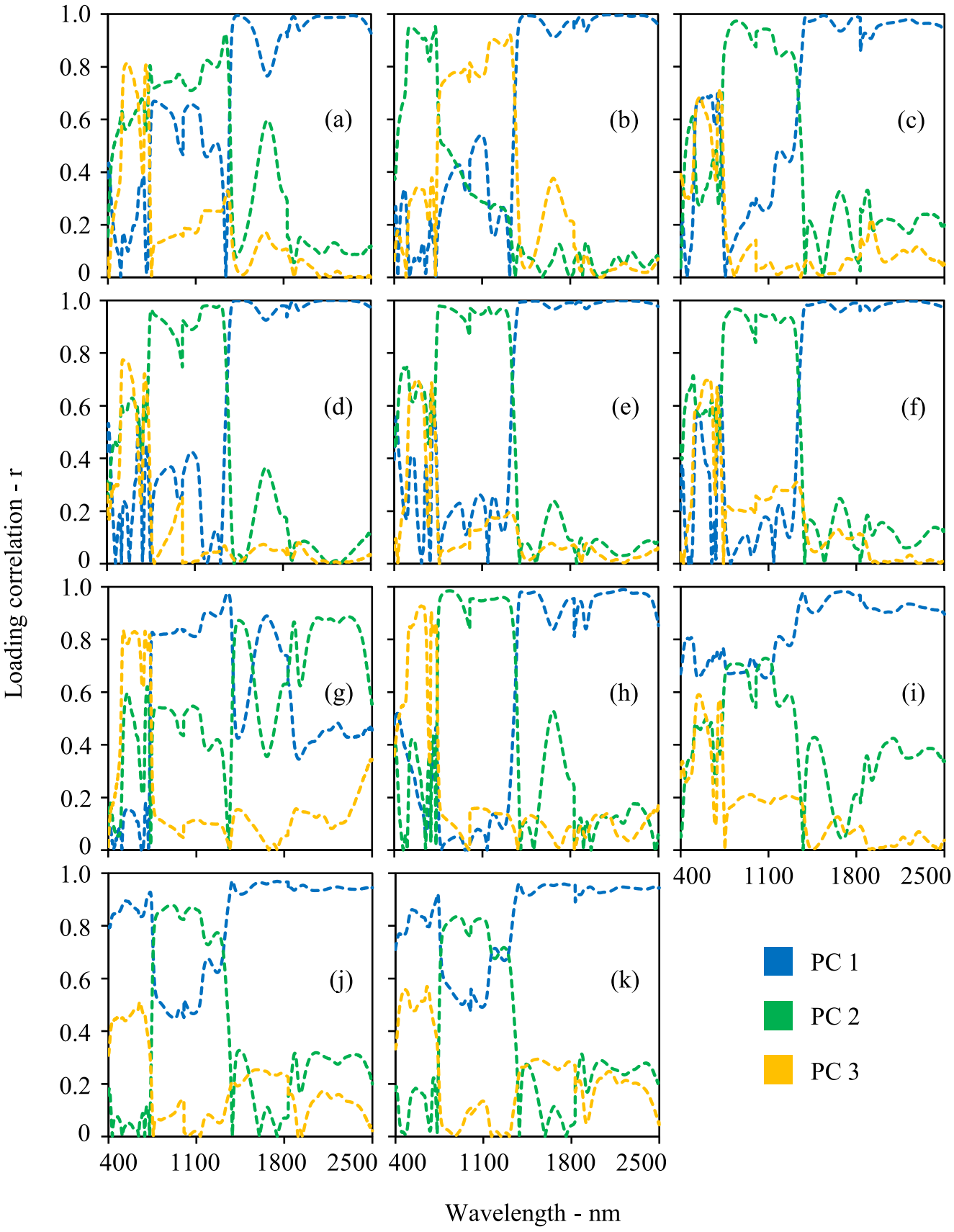


**Fig. 8.** Loading correlation of PCA of soybean reflectance under the evaluated water condition in the: 2016/2017 cropping season at 57 DAS (a) and 112 DAS (b); 2017/2018 cropping season at 57 DAS (c), 96 DAS (d), 106 DAS (e) and 112 DAS (f); 2018/2019 cropping season at 41 DAS (g), 57 DAS (h), 87 DAS (i), 101 DAS (j) and 107 DAS (k).

**Table 5**
Statistical parameters of PLSR for soil moisture prediction in the 2016/2017, 2017/2018, and 2018/2019 cropping seasons on each day of spectral assessment (expressed in days after sowing – DAS) at 0–20 cm and 20–40 cm depths.

| Depth (cm) | Cropping season | DAS | PLSR factors | $R^2_c$ | $R^2_{cv}$ | $RMSE_c$ | $RMSE_{cv}$ | $BIAS_{cv}$ |
|---|---|---|---|---|---|---|---|---|
| 0–20 | 2016/2017 | 57 | 10 | 0.938 | 0.858 | 0.902 | 1.392 | -0.000 |
| | | 112 | 5 | 0.702 | 0.623 | 2.072 | 2.370 | 0.050 |
| | 2017/2018 | 57 | 4 | 0.332 | 0.230 | 1.479 | 1.607 | 0.006 |
| | | 96 | 10 | 0.899 | 0.829 | 1.250 | 1.646 | 0.031 |
| | | 106 | 9 | 0.900 | 0.817 | 1.329 | 1.818 | 0.022 |
| | | 112 | 11 | 0.882 | 0.792 | 1.038 | 1.365 | -0.000 |
| | 2018/2019 | 41 | 4 | 0.308 | 0.212 | 0.668 | 0.722 | 0.009 |
| | | 57 | 14 | 0.779 | 0.519 | 2.105 | 3.149 | -0.054 |
| | | 87 | 8 | 0.914 | 0.860 | 1.456 | 1.881 | 0.014 |
| | | 101 | 6 | 0.766 | 0.703 | 1.186 | 1.353 | 0.011 |
| | | 107 | 6 | 0.713 | 0.618 | 1.661 | 1.941 | 0.022 |
| 20–40 | 2016/2017 | 57 | 10 | 0.940 | 0.871 | 0.855 | 1.273 | -0.023 |
| | | 112 | 10 | 0.851 | 0.674 | 1.120 | 1.688 | -0.020 |
| | 2017/2018 | 57 | 6 | 0.602 | 0.492 | 1.028 | 1.176 | 0.007 |
| | | 96 | 10 | 0.895 | 0.835 | 1.238 | 1.568 | 0.003 |
| | | 106 | 8 | 0.914 | 0.840 | 1.080 | 1.493 | 0.012 |
| | | 112 | 1 | 0.735 | 0.727 | 1.049 | 1.078 | 0.005 |
| | 2018/2019 | 41 | 1 | 0.006 | n.s. | 0.887 | 0.920 | -0.002 |
| | | 57 | 13 | 0.805 | 0.589 | 1.327 | 1.951 | -0.020 |
| | | 87 | 10 | 0.950 | 0.906 | 1.018 | 1.415 | 0.004 |
| | | 101 | 6 | 0.747 | 0.678 | 1.079 | 1.232 | 0.001 |
| | | 107 | 6 | 0.770 | 0.694 | 1.246 | 1.456 | 0.013 |

[c.] calibration step; [c.v.] cross-validation step; [n.s.] non-significant.

the low amplitude of soil moisture values (Fig. 9) and to the absence of significant differences among the water condition treatments (Fig. 4). On the other nine assessment days across the three cropping seasons, large amplitudes in soil moisture were observed (Fig. 9), and significant differences between the experimental treatments were detected (Fig. 4). Hence, at 0–20 cm depth, the $R^2$ ranged from 0.702 to 0.938 (calibration step) and from 0.519 to 0.860 (cross-validation step), with soil moisture values ranging from 18% to 35%. At 20–40 cm depth, the $R^2$ ranged from 0.735 to 0.950 (calibration step) and from 0.589 to 0.906 (cross-validation step), with soil moisture values ranging from 20% to 35%.

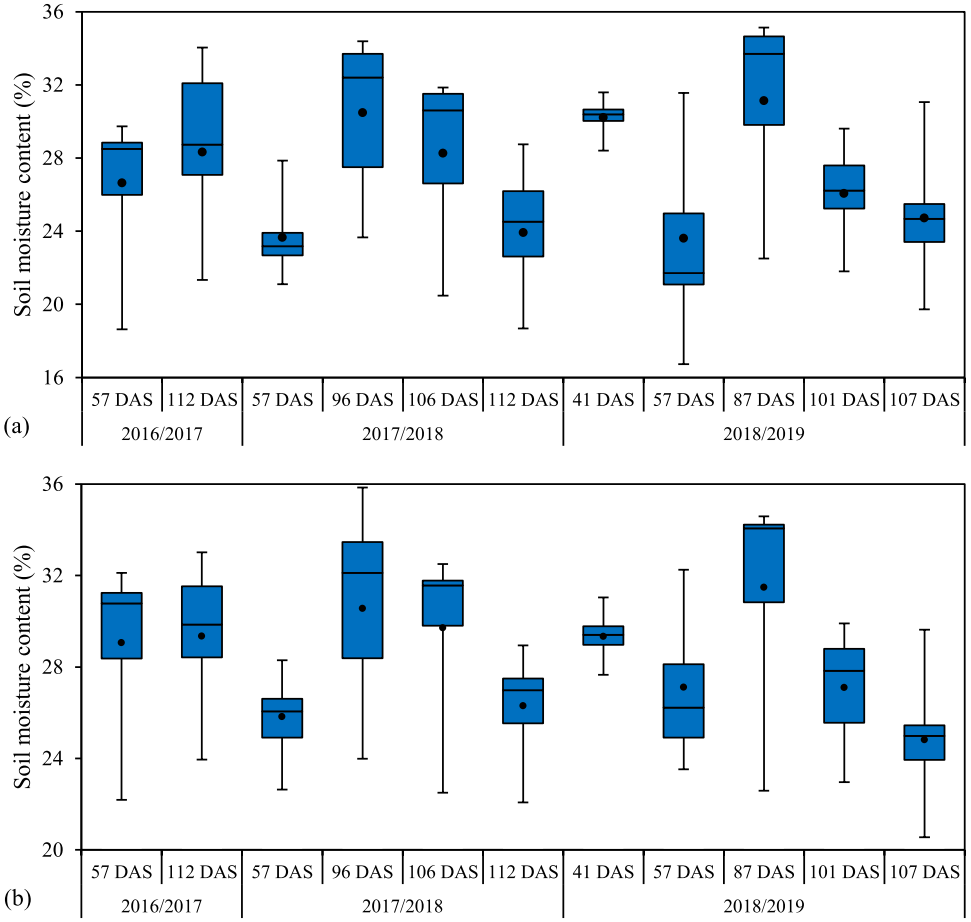


**Fig. 9.** Soil moisture at 0–20 cm (a) and 20–40 cm (b) during the 2016/2017, 2017/2018, and 2018/2019 cropping seasons.

For developing a soil moisture prediction model based on soybean leaf reflectance at different phenological stages, at 0–20 and 20–40 cm depths, we analyzed spectral and soil moisture data acquired on the eleven assessment days on the three cropping seasons into the same PLSR model. Fig. 10 presents the soil moisture values comprising all the 844 samplings (all data) and their random division into calibration/cross-validation subset (80%) and external validation subset (20%). Within each depth, the soil moisture values from each dataset demonstrated having a similar distribution. When comparing the two evaluated depths, it is possible to observe the similarity in their maximum values but with smaller minimum values at 0–20 cm depth.

Table 6 displays the results of the PLSR in the prediction of soil moisture comprising spectral data collected in the three evaluated cropping seasons (2016/2017, 2017/2018, and 2018/2019). At 0–20 cm depth, the obtained $R^2$ during the calibration and cross-validation steps was over 0.58 and RMSE lower than 2.855. At 20–40 cm depth, the PLSR model showed higher accuracy during the calibration and cross-validation steps, with $R^2$ over 0.69 and RMSE lower than 2.014.

Fig. 11 presents the regression coefficients of the PLSR model for soil moisture prediction at 0–20 cm and 20–40 cm depths. The shape of the regression coefficients curve from both depths was similar but with larger amplitudes (positive and negative peaks) observed at 20–40 cm depths. At the two evaluated depths, though the adequate distribution of PLSR coefficients across the spectrum, positive and negative sizable peaks were observed across visible wavelengths (highly influenced by the absorption of photosynthetically active radiation) and across shortwave wavelengths (deeply influenced by the leaf water content).

When applying the generated soil moisture prediction models to external samples (external validation), a positive correlation was achieved between the observed and predicted values at 0–20 cm and 20–40 cm depths, as demonstrated in Fig. 12.

The regression analysis with an intersection passing through the origin ($y = bx$) revealed, at 0–20 depth, an adjusted model ($y = 0.9948$ x) with a coefficient of determination ($R^2$) equal to 0.609. At 20–40 depth, the regression analysis with an intersection passing through the origin ($y = bx$) revealed an adjusted model ($y = 0.9958$ x) with $R^2$ equal to 0.722.

The similar accuracies ($R^2$ and RMSE), within each depth, among the calibration, cross-validation, and external validation steps, demonstrate the prediction capacity, and stability of the PLSR models, strengthening the possibility of their application to new soybean cropping areas.

The developed PLSR model based on the eleven assessment days and both depths, despite the lower accuracy compared to the PLSR models intended specifically for each assessment day (Table 5), comprises the variability from plants at different water statuses and different phenological stages across three cropping seasons, with soil moisture values ranging from 16% to 35% (0–20 cm depth) and from 20% to 35% (20–40 cm depth). Brazil has enormous variability in weather conditions (Sentelhas et al., 2015) and an extended soybean sowing calendar in each region (Kaster and Farias, 2012). That fact impairs the spectral assessment of the crop in extensive areas at the same phenological stage.

**Table 6**
Statistical parameters of PLSR for soil moisture prediction.

| | 0–20 cm | | | 20–40 cm | | |
|---|---|---|---|---|---|---|
| | $R^2$ | RMSE | BIAS | $R^2$ | RMSE | BIAS |
| Calibration | 0.589 | 2.855 | – | 0.715 | 1.928 | – |
| Cross-validation | 0.607 | 2.794 | -0.034 | 0.690 | 2.014 | -0.003 |

A soil moisture prediction model applicable throughout the cropping season would help to improve agricultural practices, resulting in better soil moisture management for optimum crop development. The contributions of the results from the present manuscript include the possible identification of zones with limitations to the development of the root zone due to soil compaction, and consequent lower levels of soil water availability to support crop development during water deficit periods, enabling the soil management in specific areas. Added to that, the methodology presented might assist the delimitation of managements zones according to the levels of soil water availability, maximizing the potential for crop production in each area and reducing the cost of production. Although irrigation represents a small percentage of soybean areas in Brazil, the definition of irrigation schedule in soybean crop might benefit from the soil moisture monitoring through leaf reflectance assessments, enlarging the percentage of irrigated soybeans in Brazil with sustainable practices, promoting the environment preservation and contributing for a larger stability of grain yield during water deficit periods.

The methodology described in the present research has large potential to be applied in different soil types. However, the coefficients of the spectral models are expected to be different in each soil type due to its physical-chemical characteristics. Therefore, spectral models for crop water status monitoring and soil moisture prediction should be developed specifically for each soil type, considering its specific edaphoclimatic characteristics, guarantying, thus, the prediction of values in accordance to the real values observed in field conditions.

### *3.4. Performance comparison of Partial Least Squares Regression with spectral bands and vegetation indices for soil moisture monitoring*

Following the soil moisture prediction, using samplings from the eleven assessment days on the three cropping seasons, results from PLSR were compared to the results from single-wavelength reflectance, hyperspectral vegetation index, and broadband reflectance and

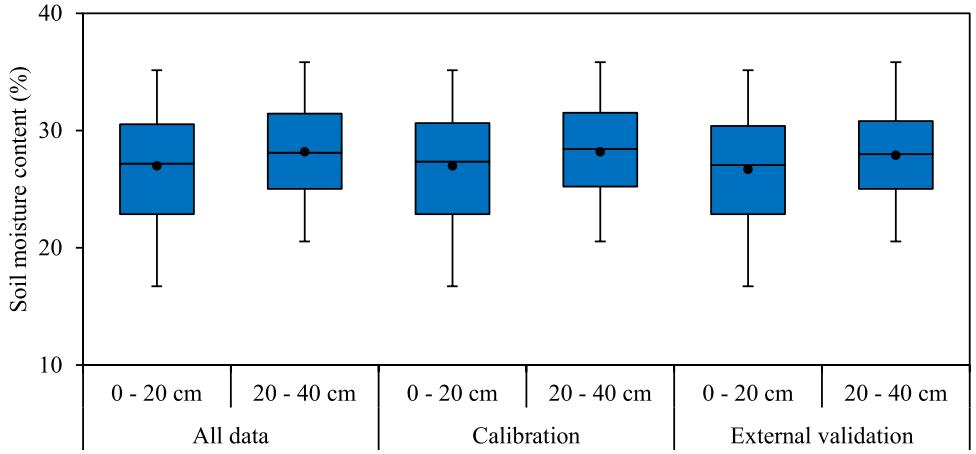


**Fig. 10.** Soil moisture values from samples collected in the 2016/2017, 2017/2018, and 2018/2019 cropping seasons.

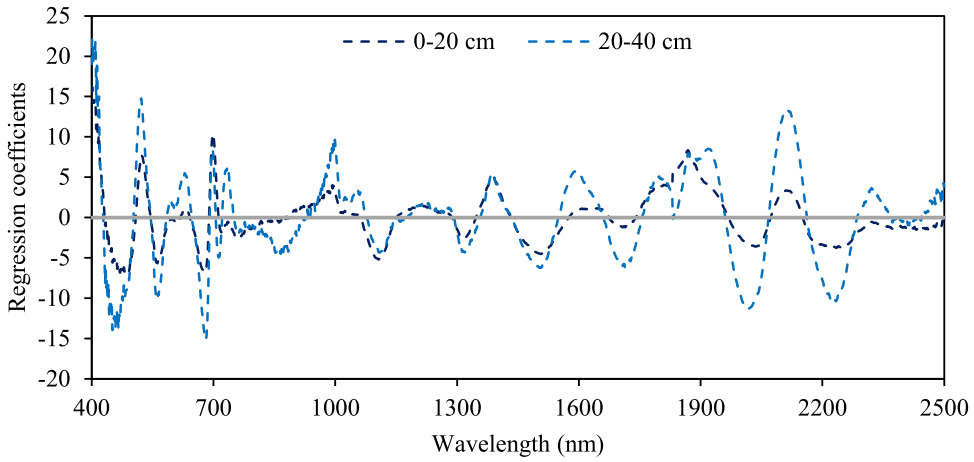


**Fig. 11.** Regression coefficients of PLSR for soil moisture prediction.

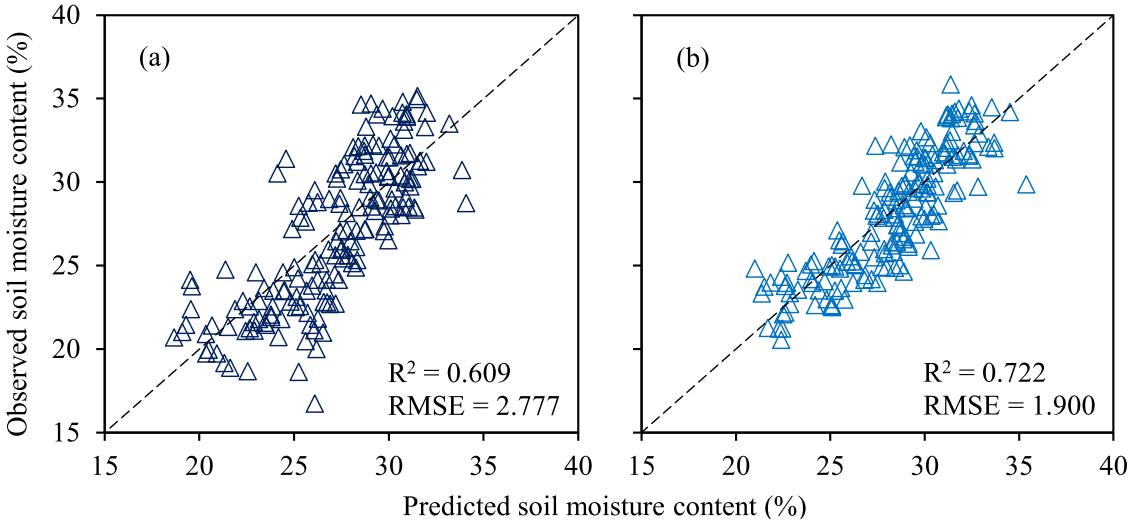


**Fig. 12.** Correlation between observed and predicted (external validation) values of soil moisture at 0–20 cm (a) and 20–40 cm (b) through PLSR (developed using 80% of data – 669 samples and validated with the remaining 20% of the data – 175 samples).

vegetation index to evaluate whether univariate linear regression based on simple spectral models can deliver competitive results.

Fig. 13 presents the coefficient of determination ($R^2$) from the calibration step (using 80% of samples) between soil moisture and: single wavelengths reflectance (a), broadband reflectance and vegetation index (b), and all possible band-to-band combinations to calculate the hyperspectral vegetation indices (c and d - Eq. 2).

Using single-wavelength reflectance across the Vis-NIR-SWIR spectrum (Fig. 13 a), the highest correlations were observed across SWIR wavelengths, followed by the Vis spectrum and NIR spectrum (the lowest correlations). The outstanding spectral bands were 1965 nm ($R^2$ = 0.335) and 1957 nm ($R^2$ = 0.331) for 0–20 cm and 20–40 cm respectively.

Using broadband reflectance and vegetation indices (Fig. 13 b), spectral bands outperformed vegetation indices, and the outstanding spectral features were the SWIR 3 ($R^2$ = 0.219) and SWIR 2 ($R^2$ = 0.219). The calculated hyperspectral vegetation indices (Fig. 13 c and d) displayed a low correlation for Vis-Vis, Vis-NIR, Vis-SWIR, and NIR-NIR band combinations, with an intermediate correlation for NIR-SWIR band combination and the highest correlations for SWIR-SWIR band combinations. The index outperformance was composed of 1878 nm and 2004 nm ($R^2$ = 0.418) at 0–20 cm, and by 2065 nm and 2067 nm ($R^2$ = 0.405).

Fig. 14 presents the results from the external validation step (spectral models developed during the calibration step applied to the remaining 20% of data) using the univariate regression models. All strategies using univariate linear regression from a simple spectral model demonstrated to underperform the use of all spectral bands under the Partial Least Squares Regression. Hyperspectral sensors are a potential benchmark for spectral analysis and identification of essential absorption features associated with agronomic traits, to be transferred later to multispectral sensors (Prey and Schmidhalter, 2019). Our results demonstrated that the PLSR has higher accuracy ($R^2$ over 0.60) than the other methods tested ($R^2$ under 0.41).

broadband reflectance and vegetation index, and hyperspectral vegetation indices.

According to Sakamoto (2020), broadband vegetation indices are usually derived from satellite images to assess their direct relationship to biomass and infer the indirect relationship between biomass and crop traits, such as soil moisture. Since the PLSR and univariate models were developed using leaf-based reflectance, without external interferences (solar light, atmosphere conditions, and canopy background, recognized the effect of the development of spectral models – Liu et al., 2015, Ma et al., 2019), the vegetation indices performed poorly compared to the other models. Besides that, Cao et al. (2015) have shown that the larger the bandwidth, the weaker the correlation with plant water-related

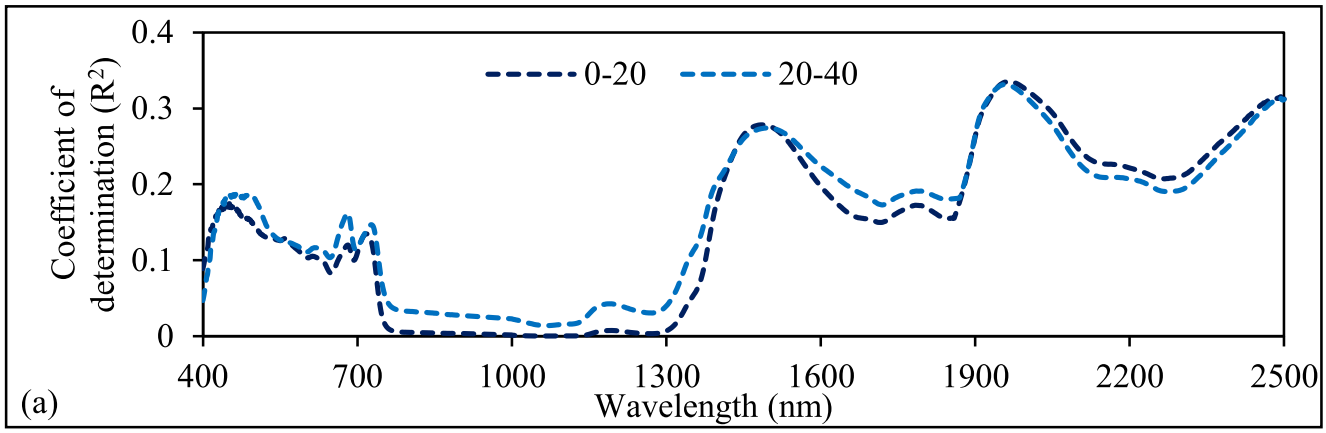


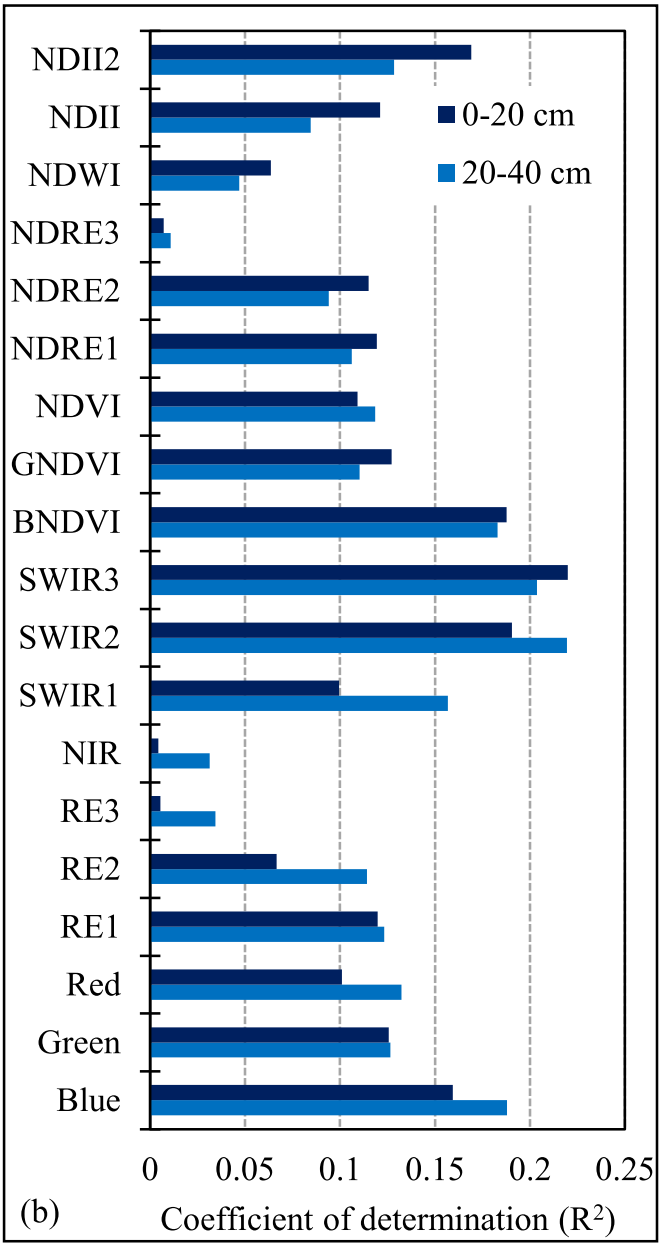


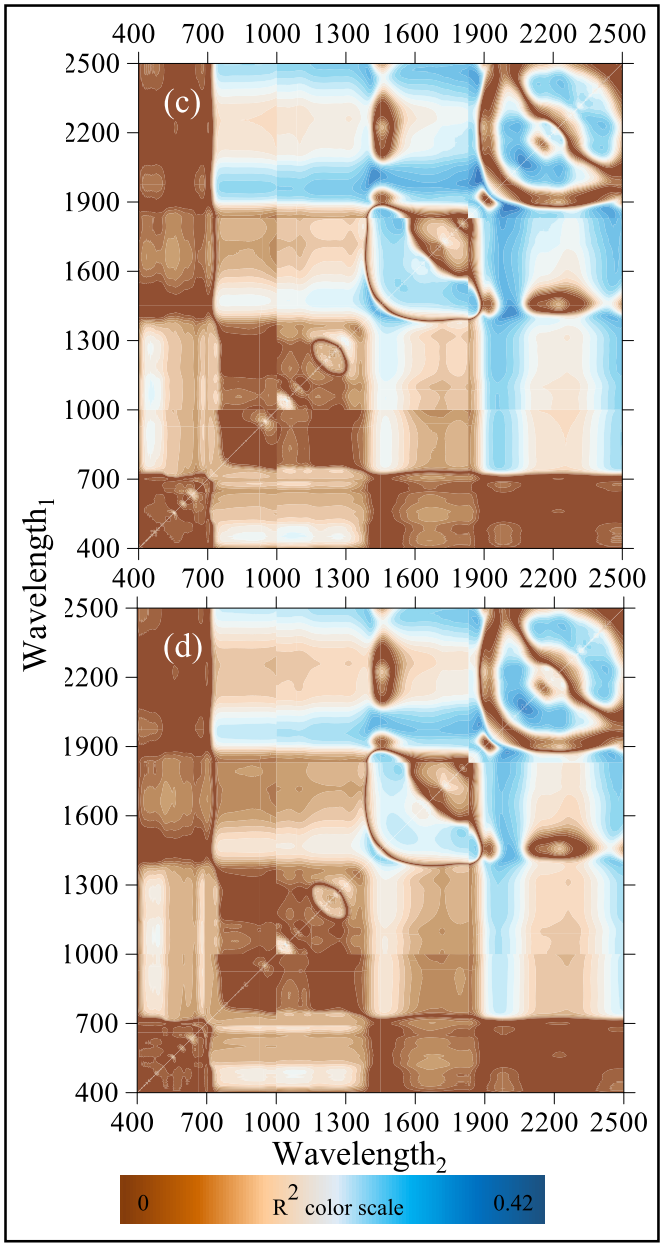


**Fig. 13.** Correlation between soil moisture and single wavelengths reflectance (a), broadband reflectance and vegetation index (b), and hyperspectral vegetation indices at 0–20 cm (c) and 20–40 cm (d) using the calibration dataset.

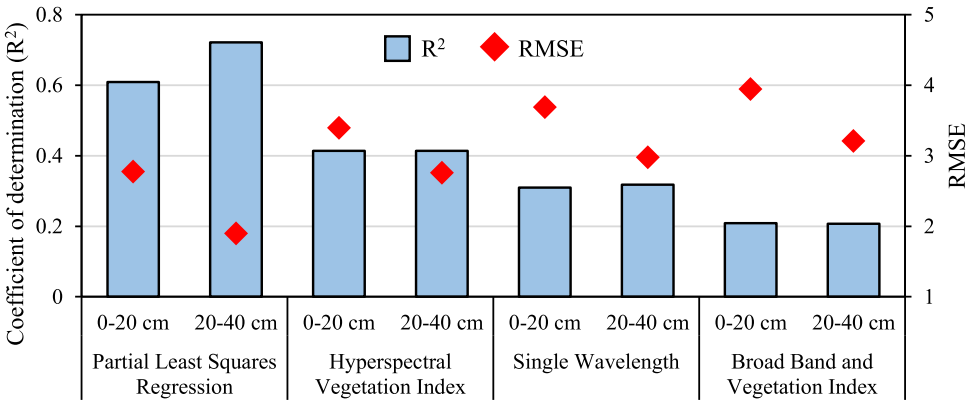


**Fig. 14.** Correlation between observed and predicted (external validation) values of soil moisture at 0–20 cm and 20–40 cm using PLSR, single wavelengths reflectance,.

properties due to spectral information loss (Mirzaie et al., 2014).

While hyperspectral vegetation indices avoid losses of spectral information contained in broadband data and have the advantage of detecting spectral features related to vegetation biophysical properties, being more suitable than the use of single wavelengths (Ge et al., 2019b; Shu et al., 2021; Zhang et al., 2012), PLSR is an efficient multivariate and machine learning regression method since it deals with multicollinearity, usually found in spectral data. The model also enables the simultaneous use of hundreds of spectral bands into the same model, weighting each one of them according to their contribution as key spectral features to predict the crop trait (Inoue et al., 2012, 2017). Thus, PLSR outperformed the broadband reflectance and vegetation indices, single wavelength reflectance and hyperspectral vegetation indices for monitoring water-related properties in several plant species (Ullah et al., 2014; Mirzaie et al., 2014; El-Hendawy et al., 2019; Ge et al., 2019b).

## 4. Conclusion

This research quantitatively monitored the soil moisture at 0–20 cm and 20–40 cm depths in a soybean field using leaf-based hyperspectral reflectance. Based on the effects of water condition treatments on soybean leaf reflectance, the Principal Component Analysis (PCA) contributed to the clustering of the experimental treatments, especially when the water deficit is during the soybean reproductive phase, the highest contribution of shortwave infrared wavelengths to crop water status monitoring.

The Partial Least Squares Regression (PLSR) demonstrated efficiency for predicting soil moisture, admitting the poor performance observed under the absence of significant soil moisture differences between water conditions. The PLSR models developed using samples from all assessment days across the three cropping seasons presented $R^2$ of 0.607 (0–20 cm) and 0.690 (20–40 cm) in the cross-validation step, and $R^2$ of 0.609 (0–20 cm) and 0.722 (20–40 cm) in the external validation step, with RMSE of 2.7 and 1.9 at 0–20 cm and 20–40 cm depths, respectively.

A remarkable outperformance of the PLSR was observed when using the entire soybean leaf spectra (Vis-NIR-SWIR) in the calibration and external validation steps compared to traditional univariate regression methods (single wavelength reflectance, hyperspectral vegetation index, and broadband reflectance and vegetation index), emphasizing the contribution of hyperspectral data in the quantitative monitoring of soil moisture in soybean areas.

While most publications address soil moisture monitoring based on qualitative and indirect measurements, this article demonstrates the potential of developing spectral models capable of quantitatively describing the levels of water availability for plants under field conditions. The present methodology enhances the possibility of applying spectral models for soil moisture assessment in extended soybean areas regardless of their stage of development. That constitutes a distinguished contribution since, in Brazil, the sowing calendar might present differences of over 30 days within the same production region and rarely with plants at the same phenological stage.

## Declaration of Competing Interest

The authors declare that they have no known competing financial interests or personal relationships that could have appeared to influence the work reported in this paper.

## Data Availability

Data will be made available on request.

## Acknowledgements

This manuscript is part of a technical and institutional cooperation program between the Central Bank of Brazil (BCB), the Ministry of Agriculture, Livestock and Food Supply (MAPA), the Brazilian Agricultural Research Corporation (Embrapa) and the Foundation for Research and Development Support (FAPED). This manuscript was approved for publication by the Editorial Board of Embrapa Soja (National Soybean Research Center – Brazilian Agricultural Research Corporation) as manuscript number 188/2022.

## Appendix A. Supporting information

Supplementary data associated with this article can be found in the online version at doi:10.1016/j.agwat.2022.108089.

## References

Alvares, C.A., Stape, J.L., Sentelhas, P.C., Gonçalves, J.D.M., Sparovek, G., 2013. Köppen's climate classification map for Brazil. Meteorol. Z. 22 (6), 711–728. https://doi.org/10.1127/0941-2948/2013/0507.

AnonUSDA (United States Department of Agriculture) – Natural Resources Conservation Service, 1999. Soil Taxonomy: A Basic System of Soil Classification for Making and Interpreting Soil Surveys. USDA: Washington, DC, USA, 1999. https://doi.org/10.1007/s100219900100.

AnonFAO (Food and Agriculture Organization of the United Nations), 2017. Agricultura Irrigada Sustentável no Brasil: Identificação de Áreas Prioritárias. Brasília. 243 p. https://gia.org.br/portal/produto/fao-agricultura-irrigada-sustentavel-no-brasil-identificacao-de-areas-prioritarias-livro-digital-pdf (Accessed 30 June 2022).

AnonFAO (Food and Agriculture Organization of the United Nations), 2018. The future of food and agriculture – Alternative pathways to 2050. Summary version. Rome. 60 pp. Licence: CC BY-NC-SA 3.0 IGO. http://www.fao.org/3/I8429EN/i8429en.pdf (Accessed 31 March 2021).

AnonESA – The European Space Agency., 2021. Sentinel-2 User Guide. https://sentinels.copernicus.eu/web/sentinel/user-guides/sentinel-2-msi (Accessed 31 March 31 2021).

AnonUSDA (United States Department of Agriculture). World Agricultural Production. Circular Series WAP 1–22, January 2022. https://apps.fas.usda.gov/psdonline/circulars/production.pdf (Accessed 18 January 2022).

AnonCONAB (National Company of Food Supply). Brazilian Crop Assessment–Grain, 2021/2022 Crops, Fourth Inventory Survey, January/2022. 2022. https://www.conab.gov.br/info-agro/safras/graos/boletim-da-safra-de-graos (Accessed 18 January 2022).

Braga, P., Crusiol, L.G.T., Nanni, M.R., Caranhato, A.L.H., Fuhrmann, M.B., Nepomuceno, A.L., Neumaier, N., Farias, J.R.B., Koltun, A., Gonçalves, L.S.A., Mertz-Henning, L.M., 2021. Vegetation indices and NIR-SWIR spectral bands as a phenotyping tool for water status determination in soybean. Precis. Agric. 22 (1), 249–266. https://doi.org/10.1007/s11119-020-09740-4.

Cao, Z., Wang, Q., Zheng, C., 2015. Best hyperspectral indices for tracing leaf water status as determined from leaf dehydration experiments. Ecol. Indic. 54, 96–107. https://doi.org/10.1016/j.ecolind.2015.02.027.

Carter, G.A., 1991. Primary and secondary effects of water content on the spectral reflectance of leaves. Am. J. Bot. 78 (7), 916–924. https://doi.org/10.2307/2445170.

Crusiol, L.G.T., 2021a. Sensoriamento remoto aplicado ao monitoramento da cultura da soja (Glycine max (L.) Merrill) sob diferentes níveis de disponibilidade hídrica. Thesis, Universidade Estadual de Maringá, Maringá, Brazil.

Crusiol, L.G.T., Nanni, M.R., Furlanetto, R.H., Sibaldelli, R.N.R., Cezar, E., Sun, L., Foloni, J.S.S., Mertz-Henning, L.M., Nepomuceno, A.L., Neumaier, N., Farias, J.R.B., 2021b. Classification of soybean genotypes assessed under different water availability and at different phenological stages using leaf-based hyperspectral reflectance. Remote Sens. 13 (2), 172. https://doi.org/10.3390/rs13020172.

Damm, A., Paul-Limoges, E., Haghighi, E., Simmer, C., Morsdorf, F., Schneider, F.D., Tol, C., van der, Rascher, U., 2018. Remote sensing of plant-water relations: an overview and future perspectives. J. Plant Physiol. 227, 3–19. https://doi.org/10.1016/j.jplph.2018.04.012.

El-Hendawy, S.E., Al-Suhaibani, N.A., Elsayed, S., Hassan, W.M., Dewir, Y.H., Refay, Y., Abdella, K.A., 2019. Potential of the existing and novel spectral reflectance indices for estimating the leaf water status and grain yield of spring wheat exposed to different irrigation rates. Agric. Water Manag. 217, 356–373. https://doi.org/10.1016/j.agwat.2019.03.006.

Falcioni, R., Moriwaki, T., Pattaro, M., Furlanetto, R.H., Nanni, M.R., Antunes, W.C., 2020. High resolution leaf spectral signature as a tool for foliar pigment estimation displaying potential for species differentiation. J. Plant Physiol. 249, 153161 https://doi.org/10.1016/j.jplph.2020.153161.

Farias, J.R.B., Assad, E.D., Almeida, I.D., Evangelista, B.A., Lazzarotto, C., Neumaier, N., Nepomuceno, A.L., 2001. Caracterização de risco de déficit hídrico nas regiões produtoras de soja no Brasil. Revista Brasileira de Agrometeorologia, 9 (3), 415–421.

Fehr, W.R., Caviness, C.E., 1977. Stages of Soybean Development; Special Report 80. Iowa State University of Science and Technology: Ames, IA, USA.

Feng, W., Qi, S., Heng, Y., Zhou, Y., Wu, Y., Liu, W., He, L., Li, X., 2017. Canopy vegetation indices from in situ hyperspectral data to assess plant water status of winter wheat under powdery mildew stress. Front. Plant Sci. 8, 1219. https://doi.org/10.3389/fpls.2017.01219.

Ferreira, D.F., 2011. Sisvar: a computer statistical analysis system. Ciência e agrotecnologia 35, 1039–1042. https://doi.org/10.1590/S1413-70542011000600001.

Ferreira, R.C., 2016. Quantificação das Perdas por Seca na Cultura da Soja o Brasil. Ph.D. Thesis. Universidade Estadual de Londrina, Londrina, Brazil.

Fuganti-Pagliarini, R., Ferreira, L.C., Rodrigues, F.A., Molinari, H.B., Marin, S.R., Molinari, M.D., Marin, S.R., Molinari, M.D.C., Marcolino-Gomes, J., Mertz-Henning, L.M., Farias, J.R.B., Oliveira, M.C.N., de, Neumaier, N., Kanamori, N., Fujita, Y., Mizoi, J., Nakashima, K., Yamaguchi-Shinozaki, K., Nepomuceno, A.L., 2017. Characterization of soybean genetically modified for drought tolerance in field conditions. Front. Plant Sci. 8, 448. https://doi.org/10.3389/fpls.2017.00448.

Furlanetto, R.H., Nanni, M.R., Mizuno, M.S., Crusiol, L.G.T., da Silva, C.R., 2021. Identification and classification of Asian soybean rust using leaf-based hyperspectral reflectance. Int. J. Remote Sens. 42 (11), 4177–4198. https://doi.org/10.1080/01431161.2021.1890855.

Gao, B.C., 1996. NDWI—A normalized difference water index for remote sensing of vegetation liquid water from space. Remote Sens. Environ. 58 (3), 257–266. https://doi.org/10.1016/S0034-4257(96)00067-3.

Gazzoni, D.L., Dall'Agnol, A., 2018. A saga da soja: de 1050 a.C. a 2050 d.C. Embrapa Soja, Brazil, Londrina.

Ge, X., Wang, J., Ding, J., Cao, X., Zhang, Z., Liu, J., Li, X., 2019a. Combining UAV-based hyperspectral imagery and machine learning algorithms for soil moisture content monitoring. PeerJ 7, e6926. https://doi.org/10.7717/peerj.6926.

Ge, Y., Bai, G., Stoerger, V., Schnable, J.C., 2016. Temporal dynamics of maize plant growth, water use, and leaf water content using automated high throughput RGB and hyperspectral imaging. Comput. Electron. Agric. 127, 625–632. https://doi.org/10.1016/j.compag.2016.07.028.

Ge, Y., Atefi, A., Zhang, H., Miao, C., Ramamurthy, R.K., Sigmon, B., Yang, J., Schnable, J.C., 2019b. High-throughput analysis of leaf physiological and chemical traits with VIS–NIR–SWIR spectroscopy: a case study with a maize diversity panel. Plant Methods 15 (1), 1–12. https://doi.org/10.1186/s13007-019-0450-8.

Gitelson, A.A., 2019. Remote estimation of fraction of radiation absorbed by photosynthetically active vegetation: generic algorithm for maize and soybean. Remote Sens. Lett. 10 (3), 283–291. https://doi.org/10.1080/2150704X.2018.1547445.

Gitelson, A.A., Peng, Y., Arkebauer, T.J., Suyker, A.E., 2015. Productivity, absorbed photosynthetically active radiation, and light use efficiency in crops: Implications for remote sensing of crop primary production. J. Plant Physiol. 177, 100–109. https://doi.org/10.1016/j.jplph.2014.12.015.

Honna, P.T., Fuganti-Pagliarini, R., Ferreira, L.C., Molinari, M.D., Marin, S.R., de Oliveira, M.C., Farias, J.R.B., Neumaier, N., Mertz-Henning, L.M., Kanamori, N., Nakashima, K., Takasaki, H., Urano, K., Shinozaki, K., Yamaguchi-Shinozaki, K., Desidério, J.A., Nepomuceno, A.L., 2016. Molecular, physiological, and agronomical characterization, in greenhouse and in field conditions, of soybean plants genetically modified with AtGolS2 gene for drought tolerance. Mol. Breed. 36 (11), 1–17. https://doi.org/10.1007/s11032-016-0570-z.

Inoue, Y., Sakaiya, E., Zhu, Y., Takahashi, W., 2012. Diagnostic mapping of canopy nitrogen content in rice based on hyperspectral measurements. Remote Sens. Environ. 126, 210–221. https://doi.org/10.1016/j.rse.2012.08.026.

Jolliffe, I.T., Cadima, J., 2016. Principal component analysis: a review and recent developments. Philos. Trans. R. Soc. A: Math., Phys. Eng. Sci. 374 (2065), 20150202. https://doi.org/10.1098/rsta.2015.0202.

Kaster, M., Farias, J.R.B., 2012. Regionalização dos Testes de Valor de Cultivo e Uso e da Indicação de Cultivares de Soja-Terceira Aproximação. Embrapa Soja-Documentos, 2012. Embrapa Soja, Brazil, 2012,, Londrina. https://ainfo.cnptia.embrapa.br/digital/bitstream/item/54939/1/Doc-330-OL1.pdf (Accessed 15 January 2022).

Kovar, M., Brestic, M., Sytar, O., Barek, V., Hauptvogel, P., Zivcak, M., 2019. Evaluation of hyperspectral reflectance parameters to assess the leaf water content in soybean. Water 11 (3), 443. https://doi.org/10.3390/w11030443.

Latimer, P., 1958. Apparent shifts of absorption bands of cell suspensions and selective light scattering. Science 127 (3288), 29–30.

Liu, L., Zhang, S., Zhang, B., 2016. Evaluation of hyperspectral indices for retrieval of canopy equivalent water thickness and gravimetric water content. Int. J. Remote Sens. 37 (14), 3384–3399. https://doi.org/10.1080/01431161.2016.1199083.

Liu, S., Peng, Y., Du, W., Le, Y., Li, L., 2015. Remote estimation of leaf and canopy water content in winter wheat with different vertical distribution of water-related properties. Remote Sens. 7 (4), 4626–4650. https://doi.org/10.3390/rs70404626.

Ma, S., Zhou, Y., Gowda, P.H., Dong, J., Zhang, G., Kakani, V.G., Wagle, P., Chen, L., Flynn, K.C., Jiang, W., 2019. Application of the water-related spectral reflectance indices: a review. Ecol. Indic. 98, 68–79. https://doi.org/10.1016/j.ecolind.2018.10.049.

Maimaitiyiming, M., Miller, A.J., Ghulam, A., 2016. Discriminating spectral signatures among and within two closely related grapevine species. Photogramm. Eng. Remote Sens. 82 (1), 51–62. https://doi.org/10.14358/PERS.82.2.51.

Marinho, J.P., Kanamori, N., Ferreira, L.C., Fuganti-Pagliarini, R., Carvalho, J.D.F.C., Freitas, R.A., Marin, S.R.R., Rodrigues, F.A., Mertz-Henning, L.M., Farias, J.R.B., Neumaier, N., Oliveira, M.C.N., de, Marcelino-Guimarães, F.C., Yoshida, T., Fujita, Y., Yamaguchi-Shinozaki, K., Nakashima, K., Nepomuceno, A.L., 2016. Characterization of molecular and physiological responses under water deficit of genetically modified soybean plants overexpressing the AtAREB1 transcription factor. Plant Mol. Biol. Report. 34 (2), 410–426. https://doi.org/10.1007/s11105-015-0928-0.

Mirzaie, M., Darvishzadeh, R., Shakiba, A., Matkan, A.A., Atzberger, C., Skidmore, A., 2014. Comparative analysis of different uni-and multi-variate methods for estimation of vegetation water content using hyper-spectral measurements. Int. J. Appl. Earth Obs. Geoinf. 26, 1–11. https://doi.org/10.1016/j.jag.2013.04.004.

Nepomuceno, A.L., Balbinot Junior, A.A., Rufino, C.F.G., Debiasi, H., Nogueira, M.A., Franchini, J.C., Alves, F.V., Almeida, R.G., de, Bungenstab, D.J., Dall'Agnol, V.F., 2021. LCS Program – Low Carbon Soybean: a new concept of sustainable soybean. Embrapa Soja Brazil, 2021, Londrina. https://ainfo.cnptia.embrapa.br/digital/bitstream/item/223611/1/COMUNICADO-TECNICO-101.pdf (Accessed 15 January 2022).

Panigrahi, N., Das, B.S., 2018. Canopy spectral reflectance as a predictor of soil water potential in rice. Water Resour. Res. 54 (4), 2544–2560. https://doi.org/10.1002/2017WR021494.

Peng, J., Shen, H., He, S.W., Wu, J.S., 2013. Soil moisture retrieving using hyperspectral data with the application of wavelet analysis. Environ. Earth Sci. 69 (1), 279–288. https://doi.org/10.1007/s12665-012-1955-x.

Peng, Y., Fan, M., Song, J., Cui, T., Li, R., 2018. Assessment of plant species diversity based on hyperspectral indices at a fine scale. Sci. Rep. 8 (1), 1–11. https://doi.org/10.1038/s41598-018-23136-5.

Prey, L., Schmidhalter, U., 2019. Simulation of satellite reflectance data using high-frequency ground based hyperspectral canopy measurements for in-season estimation of grain yield and grain nitrogen status in winter wheat. ISPRS J. Photogramm. Remote Sens. 149, 176–187. https://doi.org/10.1016/j.isprsjprs.2019.01.023.

do Rio, A., Sentelhas, P.C., Farias, J.R.B., Sibaldelli, R.N., Ferreira, R.C., 2016. Alternative sowing dates as a mitigation measure to reduce climate change impacts on soybean yields in southern Brazil. Int. J. Climatol. 36 (11), 3664–3672. https://doi.org/10.1002/joc.4583.

Rolla, A.A.D.P., Carvalho, J.D.F.C., Fuganti-Pagliarini, R., Engels, C., Do Rio, A., Marin, S.R.R., de Oliveira, M.C.N., Beneventi, M.A., Marcelino-Guimarães, F.C., Farias, J.R.B., Neumaier, N., Nakashima, K., Yamaguchi-Shinozaki, K., Nepomuceno, A.L., 2014. Phenotyping soybean plants transformed with rd29A:AtDREB1A for drought tolerance in the greenhouse and field. Transgenic Res. 23 (1), 75–87. https://doi.org/10.1007/s11248-013-9723-6.

Sakamoto, T., 2020. Incorporating environmental variables into a MODIS-based crop yield estimation method for United States corn and soybeans through the use of a random forest regression algorithm. ISPRS J. Photogramm. Remote Sens. 160, 208–228. https://doi.org/10.1016/j.isprsjprs.2019.12.012.

Sentelhas, P.C., Battisti, R., Câmara, G.M.S., Farias, J.R.B., Hampf, A.C., Nendel, C., 2015. The soybean yield gap in Brazil–magnitude, causes and possible solutions for sustainable production. J. Agric. Sci. 153 (8), 1394–1411. https://doi.org/10.1017/S0021859615000313.

Shu, M., Shen, M., Zuo, J., Yin, P., Wang, M., Xie, Z., Tang, J., Wang, R., Li, B., Yang, X., Ma, Y., 2021. The Application of UAV-Based Hyperspectral Imaging to Estimate Crop Traits in Maize Inbred Lines. Plant Phenomics 2021. https://doi.org/10.34133/2021/9890745.

Sibaldelli, R.N.R., Farias, J.R.B., 2017. Boletim Agrometeorológico da Embrapa Soja, Londrina, PR–2016. Embrapa Soja, Brazil 2017,, Londrina. http://www.infoteca.cnptia.embrapa.br/infoteca/handle/doc/1067152 (Accessed 15 June 2020).

Sibaldelli, R.N.R., Farias, J.R.B., 2018. Boletim Agrometeorológico da Embrapa Soja, Londrina, PR–2017. Embrapa Soja, Brazil, 2018,, Londrina. https://www.infoteca.cnptia.embrapa.br/infoteca/handle/doc/1087963 (Accessed 15 June 2020).

Sibaldelli, R.N.R., Farias, J.R.B., 2019. Boletim Agrometeorológico da Embrapa Soja, Londrina, PR–2018. Embrapa Soja, Brazil, 2019, Londrina. https://www.infoteca.cnptia.embrapa.br/infoteca/bitstream/doc/1109091/1/DOC4111.pdf (Accessed 15 June 2020).

Singer, J.W., Meek, D.W., Sauer, T.J., Prueger, J.H., Hatfield, J.L., 2011. Variability of light interception and radiation use efficiency in maize and soybean. Field Crops Res. 121 (1), 147–152. https://doi.org/10.1016/j.fcr.2010.12.007.

Sobrino, J.A., Franch, B., Mattar, C., Jiménez-Muñoz, J.C., Corbari, C., 2012. A method to estimate soil moisture from Airborne Hyperspectral Scanner (AHS) and ASTER data: Application to SEN2FLEX and SEN3EXP campaigns. Remote Sens. Environ. 117, 415–428. https://doi.org/10.1016/j.rse.2011.10.018.

Souza, A.M.D., Breitkreitz, M.C., Filgueiras, P.R., Rohwedder, J.J.R., Poppi, R.J., 2013. Experimento didático de quimiometria para calibração multivariada na determinação de paracetamol em comprimidos comerciais utilizando espectroscopia no infravermelho próximo: um tutorial, parte II. Quím. Nova 36 (7), 1057–1065. https://doi.org/10.1590/S0100-40422013000700022.

Stolf-Moreira, R., Lemos, E.G., Carareto-Alves, L., Marcondes, J., Pereira, S.S., Rolla, A. A., Pereira, R.M., Neumaier, N., Binneck, E., Abdelnoor, R.V., de Oliveira, M.C.N., Marcelino, F.C., Farias, J.R.B., Nepomuceno, A.L., 2011. Transcriptional profiles of roots of different soybean genotypes subjected to drought stress. Plant Mol. Biol. Report. 29 (1), 19–34. https://doi.org/10.1007/s11105-010-0203-3.

Streher, A.S., da Silva Torres, R., Morellato, L.P.C., Silva, T.S.F., 2020. Accuracy and limitations for spectroscopic prediction of leaf traits in seasonally dry tropical environments. Remote Sens. Environ. 244, 111828 https://doi.org/10.1016/j.rse.2020.111828.

Thornthwaite, C.W., Mather, J.R., 1955. The Water Balance; Laboratory of Climatology: Centerton, AR, USA.

Ullah, S., Skidmore, A.K., Ramoelo, A., Groen, T.A., Naeem, M., Ali, A., 2014. Retrieval of leaf water content spanning the visible to thermal infrared spectra. ISPRS J. Photogramm. Remote Sens. 93, 56–64. https://doi.org/10.1016/j.isprsjprs.2014.04.005.

Wang, L., Qu, J.J., 2007. NMDI: A normalized multi-band drought index for monitoring soil and vegetation moisture with satellite remote sensing. Geophys. Res. Lett. 34 (20) https://doi.org/10.1029/2007GL031021.

Wijewardana, C., Alsajri, F.A., Irby, J.T., Krutz, L.J., Golden, B., Henry, W.B., Gao, W., Reddy, K.R., 2019. Physiological assessment of water deficit in soybean using midday leaf water potential and spectral features. J. Plant Interact. 14 (1), 533–543. https://doi.org/10.1080/17429145.2019.1662499.

Wrege, M.S., Steinmetz, S., Reiser Júnior, C., de Almeida, I.R., 2012. Atlas climático da região sul do Brasil: estados do Paraná. St. Catarina e Rio Gd. do Sul. Pelota.: Embrapa Clima Temperado; Colombo.: Embrapa Florestas 2012.

Xu, C., Zeng, W., Huang, J., Wu, J., Van Leeuwen, W.J., 2016. Prediction of soil moisture content and soil salt concentration from hyperspectral laboratory and field data. Remote Sens. 8 (1), 42. https://doi.org/10.3390/rs8010042.

Yendrek, C.R., Tomaz, T., Montes, C.M., Cao, Y., Morse, A.M., Brown, P.J., Mcintyre, L. M., Leakey, A.D.B., Ainsworth, E.A., 2017. High-throughput phenotyping of maize leaf physiological and biochemical traits using hyperspectral reflectance. Plant Physiol. 173 (1), 614–626. https://doi.org/10.1104/pp.16.01447.

Yi, Q.X., Bao, A.M., Wang, Q., Zhao, J., 2013. Estimation of leaf water content in cotton by means of hyperspectral indices. Comput. Electron. Agric. 90, 144–151. https://doi.org/10.1016/j.compag.2012.09.011.

Yuan, J., Wang, X., Yan, C.X., Wang, S.R., Ju, X.P., Li, Y., 2019. Soil moisture retrieval model for remote sensing using reflected hyperspectral information. Remote Sens. 11 (3), 366. https://doi.org/10.3390/rs11030366.

Zhang, J., Zhang, W., Xiong, S., Song, Z., Tian, W., Shi, L., Ma, X., 2021. Comparison of new hyperspectral index and machine learning models for prediction of winter wheat leaf water content. Plant Methods 17 (1), 1–14. https://doi.org/10.1186/s13007-021-00737-2.

Zhang, L., Zhou, Z., Zhang, G., Meng, Y., Chen, B., Wang, Y., 2012. Monitoring the leaf water content and specific leaf weight of cotton (Gossypium hirsutum L.) in saline soil using leaf spectral reflectance. Eur. J. Agron. 41, 103–117. https://doi.org/10.1016/j.eja.2012.04.003.

Zhang, Z., Tang, B.H., Li, Z.L., 2019. Retrieval of leaf water content from remotely sensed data using a vegetation index model constructed with shortwave infrared reflectances. Int. J. Remote Sens. 40 (5–6), 2313–2323. https://doi.org/10.1080/01431161.2018.1471553.

Zhou, Z., Morel, J., Parsons, D., Kucheryavskiy, S.V., Gustavsson, A.M., 2019. Estimation of yield and quality of legume and grass mixtures using partial least squares and support vector machine analysis of spectral data. Comput. Electron. Agric. 162, 246–253. https://doi.org/10.1016/j.compag.2019.03.038.

Zygielbaum, A.I., Gitelson, A.A., Arkebauer, T.J., Rundquist, D.C., 2009. Non-destructive detection of water stress and estimation of relative water content in maize. Geophys. Res. Lett. 36 (12) https://doi.org/10.1029/2009GL038906.